FACULTY OF SCIENCE
UNIVERSITY OF COPENHAGEN

MSc Geophysics

A new reconstruction of climatic impurities in the Sub-Antarctic region

Continuous Flow Analysis of the SubICE firn cores: Mertz, Siple, Bouvet, Peter-First, Young

Author Estelle L. Ngoumtsa
Main Supervisors Helle Astrid Kjær and Paul Vallelonga
Co-Supervisor Anders Svennson

Abstract

Paleoclimatic records from the Sub-Antarctic region are extremely sparse [King et al. 2019]. Investigation into this region offers a unique insight into mechanisms of Southern Hemisphere climate that are not yet well understood. This thesis details impurity reconstructions for five Sub-Antarctic firn cores, analysed by means of Continuous Flow Analysis (CFA) method. The cores were drilled during leg 2 and 3 of the Antarctic Circumpolar Expedition (ACE), and constitute the Sub-Antarctic Ice Core Expedition (SubICE). The cores are situated in ideal locations to capture changes in Circumpolar Westerly Winds (CWW) and the Antarctic Circumpolar Current (ACC); two of the key processes responsibe for the mixing and ventilation of the deep ocean. The SubICE cores: Mertz, Siple, Young, Bouvet and Peter-First were melted in the CFA system at The University of Copenhagen in June 2018. The system was setup in order to detect insoluble dust particles, Ca^{2+}, NH_4^+, H_2O_2, H^+ and electrolytic meltwater conductivity. We present a high-resolution chemical analyses of the SubICE cores on a depth scale. Where data was available, we also include stable water isotopes, melt layer profiles, MSA and Na^+ measurements provided by the British Antarctic Survey. In general, the cores exhibit vast amounts of melt and/or substantial dust deposition, in some cases, compromising the signal recorded in the lab. Despite these complexities, we hypothesise potential sources of distinct features in the data and discuss charecteristics such as accumulation, dust transport, sea ice extent and biotic influence across the islands. However, it is important to note that there is not enough evidence to make any solid claims here and further investigation is needed in these critical and fascinating locations.

Contents

1 INTRODUCTION

1.1 Scope

It is of paramount importance to further understand the interactions within the Earth's climate in order to make valid projections for the future. Earth is currently undergoing a potentially irreversible change in climate, induced by a rapid increase in atmospheric greenhouse gases since the industrial revolution [Solomon et al. 2009]. Interactions between biospheric, atmospheric and oceanic interactions are of a high degree in complexity. Solar irradiance, the most prominent force controlling these systems, plays a periodic role in controlling many climatic processes [Berger 1988]. However a plethora of studies suggest and provide evidence of human influence dominating since the 1950s [Stocker et al. 2013].

A key driving factor in scientific climate research is the importance to differentiate between the natural and anthropogenic forcing on these systems. Understanding Earth's past natural climate variability will increase reliability in projections of future climatic changes and Earth response. Fortunately, curiosity of understanding the climate, even before the global warming event was on the horizon, has led to substantial development of research methods within paleoclimatology. It is now possible to infer characteristics of past climate from many sources including, but not limited to, oceanic sediments, tree rings, coral skeletons and direct atmospheric measurements. However, the most precise measurements come from planetary ice [Ruddiman 2014].

Annual accumulation of snow deposited on ice sheets provides historic records of changing environmental conditions [Cuffey and Paterson 2010]. Ice core samples from the Earth's polar caps and glaciers act as excellent archives dating back to over 800 000 years before present in Antarctica [Jouzel et al. 2007] and over 130 000 years in Greenland [NEEM community members et al. 2013]. It is possible to extract information about numerous climatic factors at the time of deposition. These factors include temperature and accumulation variability, atmospheric trace gas composition and chemical impurities in the ice. However, this information can only be utilized to its full potential if a reliable depth-age relation is established [Rasmussen et al. 2006]. The relationship is most likely unique to the ice core in question and depends on many factors. The method for obtaining an appropriate age-depth relation can vary depending on the strength of the ice core record. If there exists distinct annual layers in the record, these can be counted using properties that vary annually, such as hydrogen peroxide or

the ratio of oxygen and hydrogen isotopes [Cuffey and Paterson 2010]. Thus, combining glaciochemical properties inferred as proxies along with temperature records from isotopic composition of the ice allows reconstructions of past climate variations [Legrand and Mayewski 1997].

Continuous methods have been developed and improved over the past several decades and utilized for reconstruction of isotope records, glaciochemistry and trace gases. In the Continuous Flow Analysis system at the University of Copenhagen, the focus is on proxies for sea storms, acidity, forest fires and biological activity. In particular, this includes Na^+, Ca^{2+}, H^+, SO_4^{2-} and NH_4^+. The system also measures insoluble dust partciles and their size distributions and the electrolytic conductivity of the meltwater (closely related to the bulk of the ion content) [*CFA Impurity Measurements* n.d.]. The continuous method used in this system is sensitive enough to produce a high resolution overview of past climate and has been used on an international scale on various locations of ice core in both Greenland and the Antarctic region. This study focuses on five shallow cores from coastal Antarctica and Sub-Antarctic islands. These areas are subject to high changes in accumulation variability and have not yet been studied in detail, henceforth the aim of this master project was to provide insight into some of the glaciochemical patterns of these regions.

1.2 Research Purpose

Several shallow ice cores were drilled as part of the international Antarctic Circumpolar Expedition (ACE) between the months of December 2016 and March 2017. These five ice cores, Mertz, Siple, Bouvet, Peter-First and Young, formulate the Sub-Antarctic Ice Core Expedition (SubICE) ice cores. The aim of this study was to reconstruct and compare impurity concentrations for the five different sites in order to answer three key questions:

1. What is the mean and varibility of the parameters measured *dust*, Ca^{2+}, NH_4^+, H_2O_2, H^+ and *conductivity* across each 5 shallow cores?

2. What do the results tell us about possible sources of such impurities and how do they differ from site to site?

3. Can we identify any significant climatic events at these sites e.g. volcanic eruptions?

This report will first describe a brief theoretical background on ice cores in climate research in Section

2, e.g. how they are used as archives, using impurity signals as proxies and past ice core research in the Sub-Antarctic region. Section 3 gives an overview of the methodology involved in drilling, processing and melting of the ice cores followed by the data processing involved to obtain the impurity deposition reconstruction. The results are shown in Section 4 followed by a discussion in Section 5 and a brief conclusion.

2 BACKGROUND THEORY

2.1 Reconstructing climate from ice cores

Ice cores from Antarctica and Greenland have provided us with a plethora of unique records of past climate and environmental change, displaying information regarding several components that comprise our climate system [Svensson 2013]. The polar regions provide a clean atmospheric environment, far away from sources of anthropogenic release, wind-blown dust and biogenic emissions from soil and vegetation. The chemical reactivity of the polar atmosphere is much less than at mid-latitudes and to this end, these regions encapsulate historic climate more accurately than most other archives [Legrand and Mayewski 1997].

With the help of atmospheric transport, information is stored in individual ice crystals that are deposited onto the ice sheets and glaciers. Snow falls onto an ice sheet on an annual basis and each year forms a layer atop the polar caps. Year-after-year the layers get buried underneath one another in chronological order, creating a distinctive signature of environmental conditions at the time of deposition. As the layers of snow form and start to thicken, the pressure exerted onto the layers below increases and compacts into firn and then ice by means of plastic deformation.

Eventally, when the density reaches 917 kgm^{-3}, all the air bubbles or water-filled passageways between the firn grains are sealed off, this is known as *pore close-off* and occurs at the *close-off depth*. Before which, the air concealed in the gaps between grains also acts as an important tool for interpereting past climate. Continuous accumulation causes the annual layers to become buried into the ice sheet and ice slowly flows horizontally. This causes the layers to move downward, thinning vertically and stretching horizontally (See Figure 1). This means an ideal place for an ice core record is near an ice divide since there is negligible horizontal flow so the deeper ice is assumed to have come from the same place it was deposited [Cuffey and Paterson 2010]. However, the most optimal place for an ice core site depends on what the scientific goals are. For example, the East Greenland Ice Core Project is located in East Greenland and the initial aim was to obtain information about how ice streams behave and hence improve understanding on how they will contribute to sea level rise. Therefore this core was drilled on the North-East Greenland Ice Stream (NEGIS) and was favourable for the project's intentions.

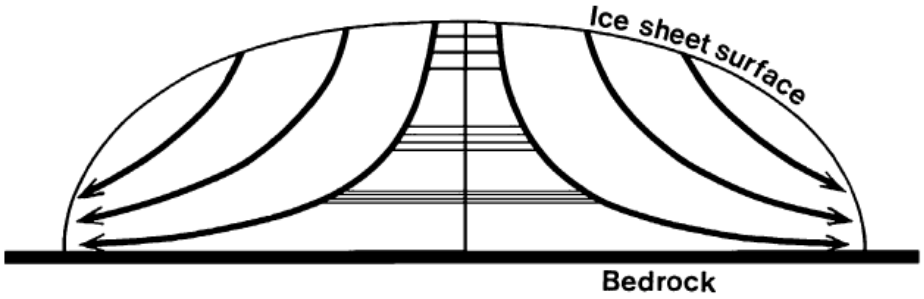

Fig. 1: This figure shows a schematic cross-section through an ice divide. Layers form atop the ice sheet and the horizontal flow of ice causes the layers to move downward and undergo glacial thinning, thinning veritcally and stretching horizontally [Svensson 2013].

In order to take full advantage of the chronological layering in an ice sheet, an age scale of the core needs to be determined. If there are visible layers in the ice then an option is to count the annual layers to determine the age of the ice. If the layers are not distinct then other methods include utilising well-dated reference horizons, glaciological modelling and orbital tuning. It is common to combine methods in order to validate the depth-age relation obtained [Cuffey and Paterson 2010].

Many useful climate components can be quantified using a wide range of methods for interpretation. Air bubbles can be analysed for concentration of carbon dioxide (CO_2), methane (CH_4) and nitrous oxide (N_2O) at the time of bubble formation. This is fundamental in climate research at present, given the uncertainties in projections of earth and ocean response to the rapid warming which is governed by such greenhouse gases [Cuffey and Paterson 2010]. Ratios of stable water isotopes, δO^{18} and δD can be measured and are directly related to local temperatures [Dansgaard and Johnsen 1969]. The heavy isotope content in precipitation decreases with condensation temperature, enabling extraction of a detailed proxy record for past temperature [Legrand and Mayewski 1997]. Glaciochemistry is an area of research focused on chemical composition of impurities in the ice. Aerosols and water soluble species are deposited directly onto the surface in the form of cloud droplets and ice crystals. Chemical impurities in ice cores will be discussed in more detail in Section 2.2. All of the records mentioned above provide a wealth of information about atmospheric forcings on past climate [Legrand and Mayewski 1997].

It is important to note that the signals are not totally free from perturbation when the information gets stored. There are uncertainties linked to the relationship between the composition of the atmosphere and the precipitation due to mixing and ventilation of volatile substances. In the upper parts of the ice sheet, gases move freely and there is exchange between the atmosphere on the surface and the pockets

of air in firn [Albert 2002]. During warmer years, there can be extended periods of melting on the surface which can have an influence on the close-off depth of air bubbles and in some cases, re-deposit information in deeper layers or melting of the entire annual signal [Kjær 2014]. Another difficulty in interpreting climate signals is distinguishing between possible causes of proxy patterns, often impurities and isotopes can act as proxies for multiple events [Cuffey and Paterson 2010].

2.2 Chemical impurities in ice

Soluble impurities can withold information about past atmopheric composition and circulation. In particular, we can infer details regarding a wide range of aerosols and the wind-borne fluxes of materials from source to site. Unlike gases such as methane and isotopes of diatomic oxygen, the lifetimes of the impurities in the atmosphere are on the order of days to weeks and therefore are not globally mixed. The impurities travel either attached to snowflakes or as independent aerosols, this is known as wet deposition and dry deposition, respectively. Aerosols directly affect the climate through alterations of the radiative balance of Earth. This is done by scattering and absorbtion of solar radiation. They also have an indirect effect when they are in the form of cloud condensation nuclei, regulating temperature changes due to varying cloud cover [Thornes 2002]. Aerosols are split into two main categories, *primary aerosols*: substances picked up by winds - e.g. continental dust and sea spray - and *secondary aerosols*: formed atmospherically by gases. However, some aerosols can adsorb onto the ice directly [Cuffey and Paterson 2010]. In this thesis, the CFA data for *dust, conductivity*, Ca^{2+}, NH_4^+, H^+ and H_2O_2 was processed and their significance will be discussed below.

Dust and sea salts

Dust, or 'microparticles' are transported by winds up through the troposphere, originating from the continental regions. Therefore they act as a paleoclimatologocial proxy for global aridity and wind strength. Dust concentrations peak with the rise in frequency and amplitude of global storms. This usually occurs in the spring and can act as an annual counting tool [Meese et al. 1997]. It is commonly acknowledged that the terrestrial dust in Northern Hemisphere cores originate from the dry regions of Asia, however in Antarctica the source is thought to be countries such as Patagonia, Argentina. In both hemispheres, the dust concentration exhibits peaks during glacial periods, mainly due to drying

and strengthening of winds in the source regions. The composition of continental dust deposition is an indication of the rock species found on the continents, most of which are particles of silicate rocks; however, some are soluble calcium carbonate $CaCO_3$ and calcium sulphate $CaSO_4$. Thus, the *dust* signal can often be driven by the Ca^{2+} content and vice versa, Ca^{2+} is usually influenced by dust. However, it is also a proxy for sea salts, amongst other ions including Na^+, Mg^{2+}, K^+, Cl^- and SO_4^{2-} [Cuffey and Paterson 2010].

It has previously been assumed that sea salt deposition was only caused by the crashing of waves and bursting of small air bubbles on the open ocean, followed by an uplift of winds to be transported onto the ice surface [Wolff et al. 2003]. However, this would cause a decrease in sea salt flux with an increase in sea ice extent. Furthermore, many now suggest that in higher latitudes, sea-salt aerosols are additionally derived from the sea ice surface [Fischer et al. 2007]. Surface tension causes upwelling of brine, which induces the formation of frost flowers onto freshly formed or submerged sea ice [Schüpbach et al. 2013]. The concentrations in these aerosols show patterns of summer minima rather than winter, thus implying its dominance when speculating sources of sea salts [Wagenbach et al. 1998].

Conductivity, acidity and sulfuric compounds

The conductivity of the meltwater can be measured in conjuction with the acidity in order to gauge the amount of electrolytic impurities in the ice [Bradley 1999]. The detection of large quantities of ions help us to indicate periods of high volcanic activity which can be used to date ice cores. These sharp peaks can also be used as marker horizons to aid the synchronization of ice cores [Svensson 2013]. The conductivity is understood as the bulk of the ionic compounds in the ice, fundamentally driven by H^+ concentrations. Acidity is defined as the inverse logarithmic activity of H^+ concenrations and arises from contributions of acidic sulfur compounds such as the acids emitted during a volcanic eruption (sulfuric acid, H_2SO_4 forming from SO_2 dissolution). The acidity can also indiciate production of CO_2 in the ice matrix [Bradley 1999]. Another important compound that will be discussed, however not measured in this study, is methane-sulfonic acid (MSA). MSA is produced by marine phytoplankton in the upper layers of the ocean, with maximum yield in the spring and summer months. This can be used as a proxy for sea ice. The sea ice retreats in the warmer periods and enhances the production of dimethylsulfide (DMS), which is released to the atmosphere and rapidly oxidises to form MSA [Abram et al. 2007]. Since this is the only known source of MSA seen in Antarctic ice cores, theories suggest

coastal ice cores could give rise to reconstructions of biogenic activity and sea ice extent [Curran et al. 2003; Abram et al. 2007].

Ammonium

Ammonium, is a biogenic aerosol emitted from the biosphere as part of the nitrogen cycle either as NH_4^+ or first as ammonia, NH_3. The main sources of which are associated with biomass combustion, bacterial decomposition in soils and vegetation cover and of excreta. It is suggested that terrestrial emissions such as above dominate the atmospheric ammonia budget [Legrand and Mayewski 1997]. Another source of ammonia could be from marine emissions [Legrand, Ducroz, et al. 1998]; although, the estimated marine budget still holds large uncertainties [Sutton et al. 1994]. In Antarctica, despite the largely oceanic proximity, the low ammonia level in the precipitation is a counter-argument to this theory of marine dominance. Anthropogenic sources of atmospheric nitrogen include the use of agricultural fertilizers, coal combustion and deforestation. Naturally, there are annual peaks in the summer where bioactivity is maximum. This creates a seasonal cycle that can be used for annual layer counting. A large amount of ammonia is released by forest fires, significantly exceeding background concentrations, hence, acting as an additional tool for dating ice cores [Legrand and Mayewski 1997].

Hydrogen peroxide

Hydrogen peroxide (H_2O_2) is widely used as a seasonality tracer in ice cores. It is mostly formed in the atmosphere by the photochemical self-reaction of hydroperoxyl radicals (HO_2) [Lamarque et al. 2011]. We see maximum concentrations during the months of higher insolation when photochemical activity is abundant. Therfore the H_2O_2 signal is commonly used to date ice cores. It is important to note that this is only possible in sites charecterized by high accumulation rates with a large summer-to-winter ratio. The method is limited to high-accumulation sites due to diffusion and smoothing effects of the seasonal cycle in the upper snow and firn. Note that this can also occur in stable isotope reconstructions. H_2O_2 is also easily destructed by terrestrial oxidants and therefore the method is not ideal for sites with high dust content [Legrand and Mayewski 1997]

2.3 Sub-Antarctic region

The SubICE core sites are located on five remote sub-Antarctic islands that had not yet been explored at the time of drilling. The unique location of the islands is subject to a great susceptibility to changes in Circumpolat Westerly Winds (CWW) and the Antarctic Circumpolar Current (ACC). These are key processes involved in the mixing and ventilation of the world's deep oceans. The aims of the drilling project were to provide reconstructions of recent changes in past climate, measure pollutants and changes in atmospheric circulation, including local wind variability [*SubICE* 2016-2019].

The Sub-Antarctic region is of particular interest for several reasons. Firstly, aerosol transport is responsible for the export of nutients to and across oceans, therefore regulating the magnitude of bioproductivity in remote regions such as the Sub-Antarctic [Boyd et al. 2000; Fischer et al. 2007]. Secondly, in the coastal regions of Antarctica, the atmosphere is highly influenced by trace gases and aerosols emitted by the surrounding oceans, hence a large marine input in climatic signals in this region [Herron et al. 1979]. This high ocean influence can be advantageous as opposed to a core site more inland where marine signals are minimal.

It can be difficult to distinguish between sources of proxies in these coastal regions, for example, sea salts originating from sea surface bubbles or changes in sea ice cover. Another example is calcium (Ca^{2+}) being driven by dust particles or sea salts. Most airborne particles follow a lognormal distribution if being transported from a single source [*Aerosol Statistics Lognormal Distributions and dN/dlogDp*]. Therefore, any deviation from this norm could suggest multiple sources for the same proxy. Another difficulty in these cores is the ability to examine seasonal vartiations due to the high complexity of the coastal aerosol signal and the multitude of surface melt [Svensson 2013].

3 METHODS

A continuous flow analysis (CFA) system is used in order to measure chemical impurities in five ice cores situated in the sub-Antarctic region. Over the course of 9 days, the firn cores: Mertz, Siple, Bouvet, Young and Peter-First were melted during a campaign held in June, in the CFA labratory at the University of Copenhagen. This section describes the methodology involved in the drilling of the cores as part of the Sub-Antarctic Circumpolar Expedition (SUBACE), followed by melting the snow/firn cores in the CFA lab before finally processing the data.

3.1 SubICE drilling project

Paleoclimate records from the Sub-Antarctic region are extremely sparse [King et al. 2019; PAGES2k Consortium et al. 2017]. The aim of the SubICE drlling expedition, directed by Liz Thomas (British Antarctic Survey), was to obtain the first climate records from glaciated Antarctic and Sub-Antarctic islands [Joel Pedro and Gaticúa n.d.]. Five unique locations were chosen for shallow core drilling around the Antarctic and sub-Antarctic region as part of the Sub-Antarctic Circumpolar Expedition (SubACE). These locations are shown in Figure 2. For all the cores, they are the first samples to be taken from their respective regions The cores range from approx. 12m - 25m in depth and characterize the climate for the past few decades. The islands are considerably remote and are located in the ideal position to capture changes in Southern Hemisphere climate, more specifically, changes in Circumpolar Westerly Winds (CWW) and the Antarctic Circumpolar Current (ACC). These are key processes responsible for the mixing and ventilation of Earth's deep oceans. The core sites vary in distance and direction from the coast, making it quite difficult for comparitive discussions between the 5 cores. Most of the information in this Section was taken from the ACE Leg 2 Report (SubACE 4 Leg 2 Report). The leg 2 route map is shown in Figure 24 in Appendix.

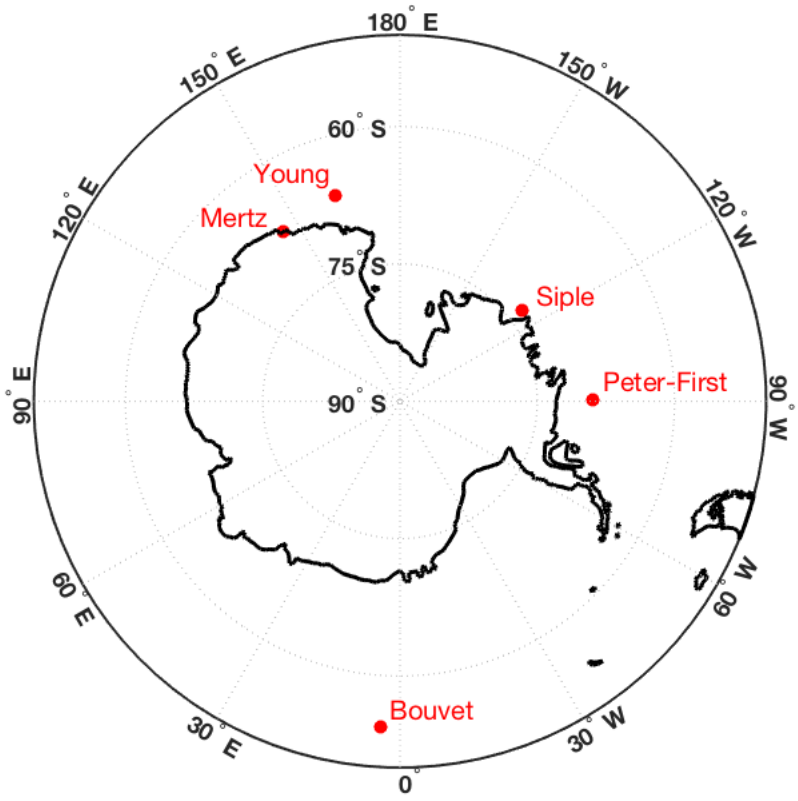

Fig. 2: Map of the Sub-Antarctic Ice Cores studied in this project. These cores were drilled during leg 2 and 3 of ACE. The Islands chosen for SubICE are highlighted in red: Bouvet Island, Peter 1st Island, Mt Siple (Siple Island), Balleny Islands (Young Island) and Mertz 1 Glacier.

Five shallow cores were drilled using a Kovacs ice core drill, powered by an electric motor. A generator is used to drive the power drill turning the drill barrel and rods, it is also used to drive the winch in order to pull up the core from the borehole. The table below displays information about the location, elevation and the depth drilled for each of the five firn cores.

Core site	**Core length (m)**	**Elevation (m)**	**Latitude (S)**	**Longitude**
Mertz 1	20.25	320	67.56	145.31 E
Young Island	16.88	238	66.53	162.56 E
Siple Island	24.14	685	73.32	126.66 W
Peter-first Island	12.29	730	68.87	90.52 W
Bouvet Island	13.84	350	54.00	3.00 E

Tab. 1: Core lengths obtained upon drilling, elevation of drill site and co-ordinates of each site.

Mertz Core (Cape Hurley)

The Mertz core was drilled on Cape Hurley, a low elevation ice dome, located East of Mertz Glacier above Fisher Bay. It is the shortest distance to the coast of Antarctica out of the 5 cores and is well suited to obtain climate and atmospheric chemistry signals from the Mertz region. The ice in this region is thought to have simple ice flow. The glacier is currently growing at a rate of 1km per year extending toward the ocean [*SPI ACE Expedition* 2016-2019]. The ice behaviour is largely influenced by bottom topography, however is still affected by local climatic changes. The site was crevasse free but the weather conditions were fairly warm upon drilling, causing the core dogs to stick occasionally. The team noticed some melt layers which were later investigated when the cores returned to the U.K at the British Antarctic Survey in Cambridge. Figure 3 shows the location where the Mertz 1 core was drilled.

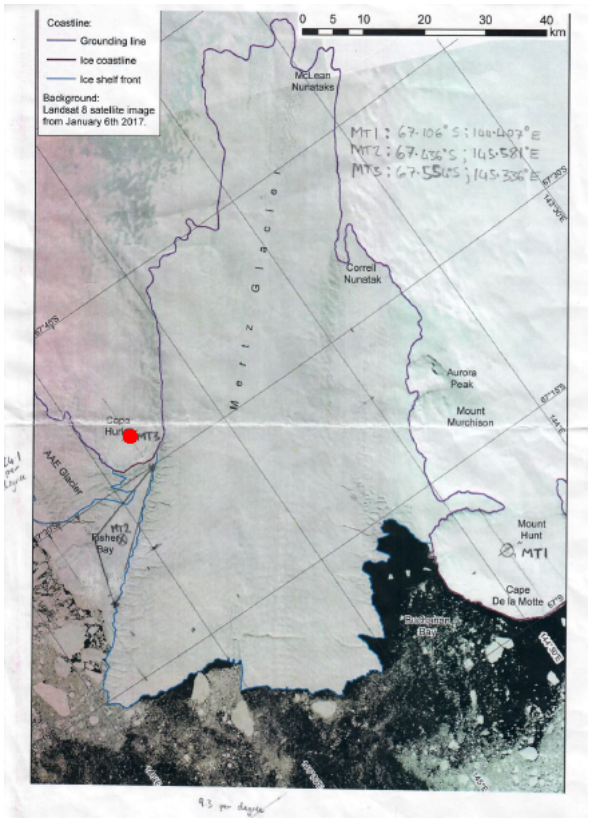

Fig. 3: Figure showing the location where the Mertz core was drilled. This is shown by the red circle, adjacent to the Mertz Glacier.

Young Island (Balleny Islands)

The Young Core site is situated in the Balleny islands, in the Antarctic seasonal sea ice zone at the boundary of the polar westerlies and coastal easterlies. After a crevasse free site was located, the drilling began. However the location was not the original desired site, due to time limitations and uncertainty in changes in cloud cover later that day. This island is most ideal for investigating past meridional shifts in the westerlies and also in regional sea ice extent [Joel Pedro and Gaticúa n.d.]. Figure 4 shows the location where the Young Island core was drilled.

Fig. 4: Figure showing the location where the Young Island core was drilled. This is shown by the red star.

Siple Island (Mt Siple)

Siple island is surrounded by Getz ice shelf. On the coast of Marie Byrd Land lies a 3110m high shield volcano, Mt. Siple. The core was drilled on the North East side of the mountain in a crevasse free, slightly sloped area between two glacier valleys. Recent studies from the Siple ice shelf show evidence of rapid thinning [Hamilton et al. 2005]. Another study from nearby ice shelves supports theories of high melt ratios and postulate strong ocean thermal forcing playing a large role in this ablation source [Rignot et al. 2013]. This is the Southern Hemisphere's region of highest climate variability, therefore a highly influencing factor contributing to West Antarctic variability and the surrounding oceanic environment [*NCAR UCAR Climate Data Guide* 2019]. Therefore, location is well suited to capture changes in the Amundsen Sea Low and the linked temperature and sea ice fluctuations, thus was the motivation for drilling on this island [Joel Pedro and Gaticúa n.d.]. Figure 5 shows the location where the Siple Island core was drilled.

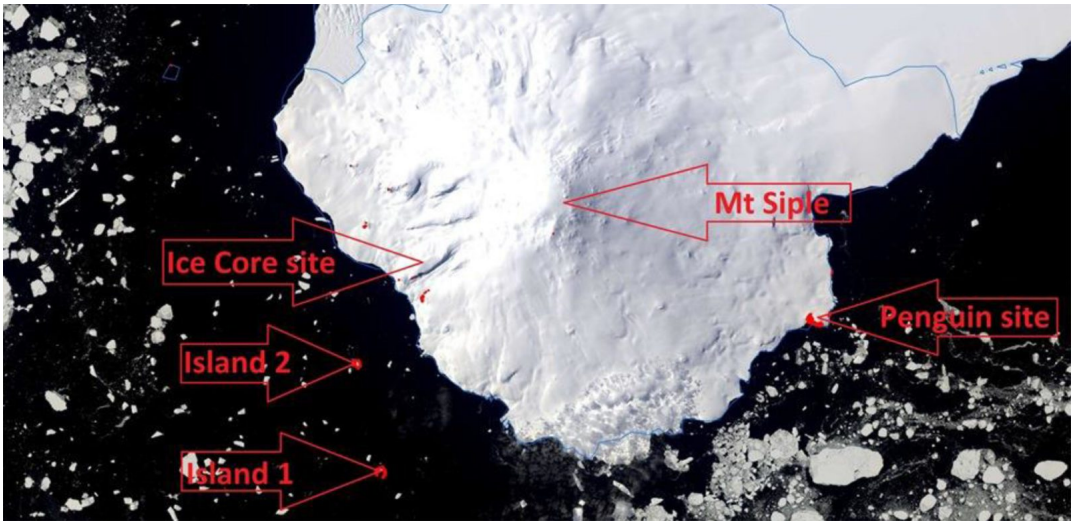

Fig. 5: Figure showing the location of Mt Siple, elevation is 3110m at the peak. The ice core site is situated on the shoulder between two glaciers North East of the mountain.

Peter-First Island

Peter 1st island is located in the seasonal sea ice zone of the Amundsen-Bellinghausen sea making it a highly desirable area of interest. It is totally covered in ice. The core was initially supposed to be drilled in a plateau at the top of the island, however, due to weather conditions, a lower elevation, non-crevassed site was chosen on the Eastern side of the island on the Midtryggen ridge. The weather conditions unfortunately caused limitations on the total depth drilled. However, no ice core has ever been obtained from this island (much like the others) therefore the drilling was still a success albeit one of the shallower cores from the project. Figure 6 shows the location where the Peter-First core was drilled.

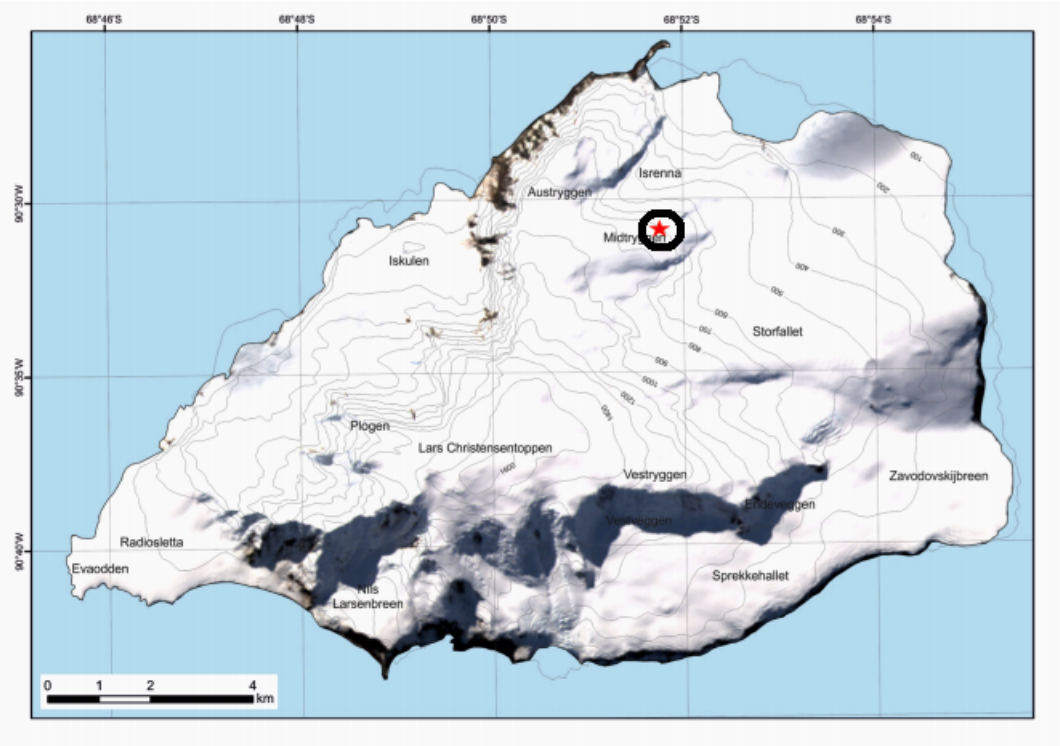

Fig. 6: Figure showing the location of Peter-First core site, marked by a red star.

Bouvet

Bouvet Island is a volcanic island which is known to be the most remote, inaccessible place on Earth. Approximately 90% of the island is covered by ice, forming steep icy walls on the island rims [*SPI ACE Expedition* 2016-2019]. The core was drilled on the eastern slope of the island at an altitude of 350m [King et al. 2019]. Unlike the other 4 cores drilled in leg 2 of the expedition, Bouvet was sampled during leg 3.

Bouvet is the only SubICE core thus far to have documented research published. King et al. 2019 interpreted records of several organic compounds alongside other chemicals more commonly measured in ice cores. Organic compounds make up 50% of the atmospheric aerosols, however this area has not been widely explored yet in ice cores. They investigated these marine biospheric compounds' ability to act as multiproxy sea ice markers in the Sub-Antarctic region. The study finds positive correlations of MSA with sea ice concentration in the Bouvet region during winter-to-spring, with the most significant correlation upon the margin of maximum sea ice extent. The correlation is likely linked to increases in phytoplankton blooming events in the spring, when sea ice concentration was larger in the preceeding winter. Some of the compounds studied require further investigation. However, oleic acid also shows strong positive correlations with MSA and sea ice conentration through the same period and region. This could be a newly found potential proxy for sea ice [King et al. 2019]. Figure 7 shows the location where the Bouvet core was drilled.

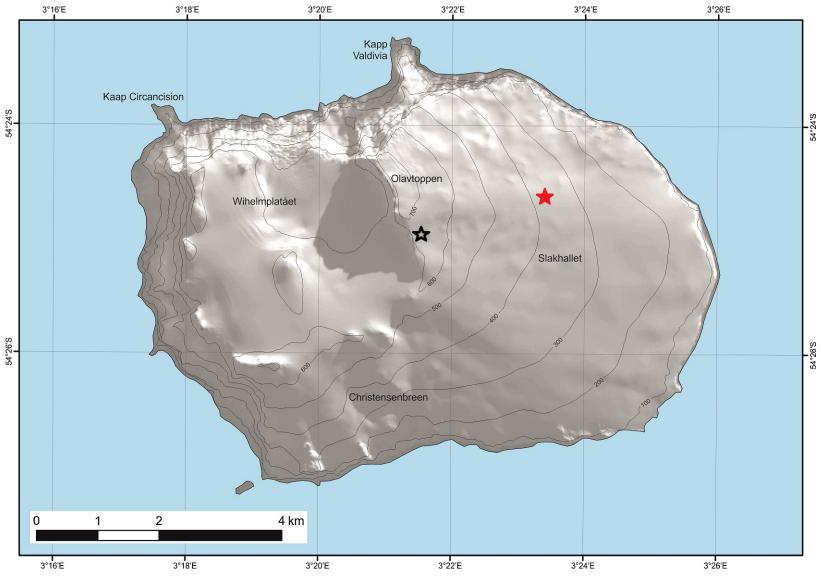

Fig. 7: Figure showing the location of Bouvet Island core site, marked by a red star.

3.2 SubICE melting campaign

Before the cores can be melted in the lab they must be carefully prepared in the ice core freezer and put in to core frames so that they are centered when approaching the melthead. After drilling, the cores were bagged in sections of approximately 60 - 80 cm in length, before putting into boxes for transportation. The firn cores are very low in density and are susceptible to damage during transport therefore need to be processed - first, they are measured and their length is noted down. They are then cut perpendicular to their cross section to obtain an area of 3.5cm x 3.5cm. The remaining sub-sections are packed away as archives for further analysis. The next step is to make sure any internal breaks are not too diagonal, so the edges need to be "shaved" until they are as horizontal as possible. This causes gaps in the data that need to be accounted for later on when converting the data onto a depth scale. Once the cores are ready they are transferred into a plexiglas frame and stored until they are ready to be melted in the CFA lab.

The SubICE cores were melted using the CFA system that was developed at the Physics of Ice, Climate and Earth department at NBI (Niels Bohr Institute), University of Copenhagen. The system is optimized for high resolution sampling with a maximum resolution of 1cm. The observed thickness of annual snow layers in the deeper parts of ice cores, such as NGRIP and GRIP, is of the order of 1cm after compression and glacial thinning has occurred [Svensson et al. 2008]. Thus, the system is able to determine transient signals in the individual layers of the ice cores, which is crucial since precipitation sources can shift in just a few years. This continous method is therefore much more favourable than discrete-sampling methods since it is much less time consuming and with a higher resolution [Bigler et al. 2011]. It is worth noting here that the SubICE cores are snow/firn cores. They are shallow cores, all less than 25m in depth, therefore they are not very dense. Hence, there is not enough accumulation on the upper layers of the core to cause much thinning below it.

CFA set up

The CFA system uses a combination of spectrometric and spectroscopic techniques in order to determine concentration of acidity (H^+ ions), sodium (Na^+), ammonium ($NH4^+$), hydrogen peroxide (H_2O_2) and calcium (Ca^{2+}) as the core is melted from the top down. The system also measures electrolytic meltwater conductivity (σ) and dust particles. Figure 3.2 shows the flowchart for the CFA set up used in the SubICE melting campaign in June 2018.

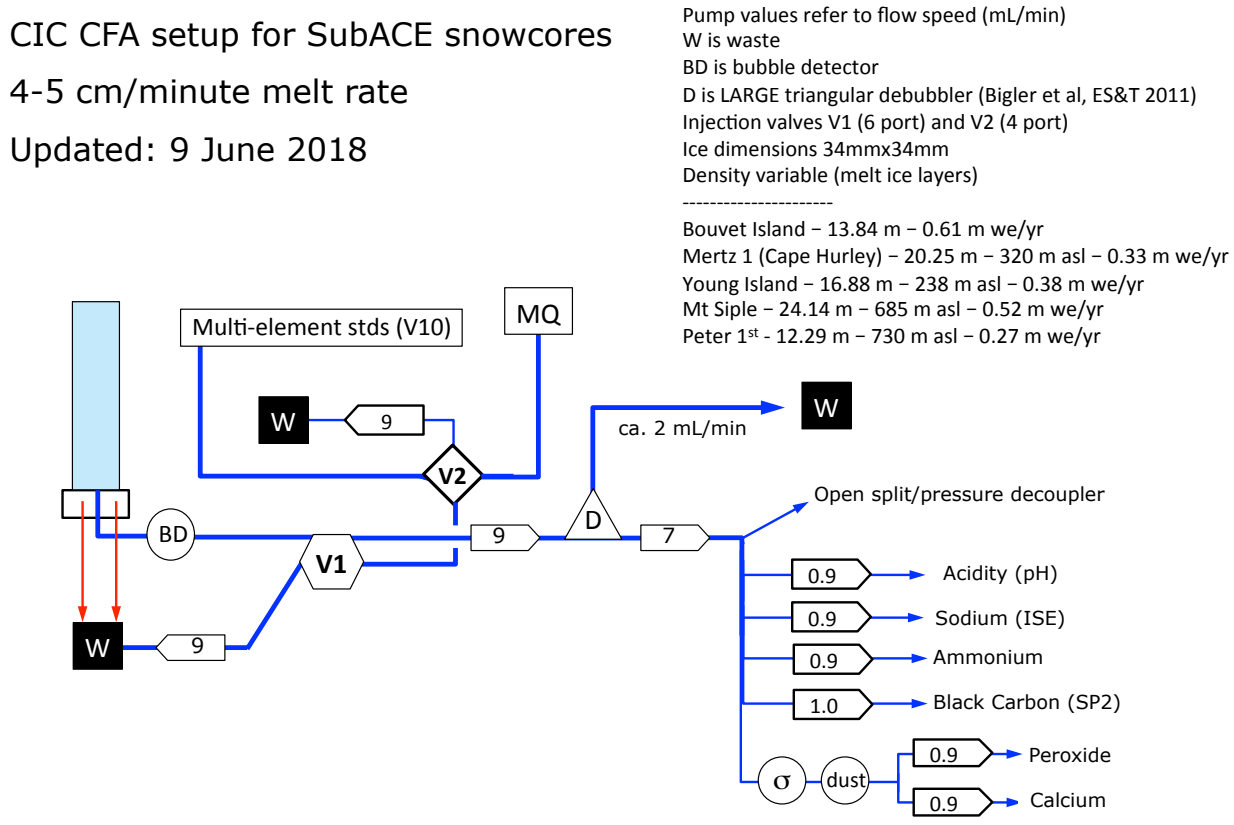

Fig. 8: From left to right: The ice core is placed in the freezer, shaded in blue. In the freezer, the ice is lowered onto the melthead whilst being held and guided by the ice core frame. As the core melts, the outer core leaves the system as waste, marked W, and the inner, uncontaminated part of the core proceeds through a bubble detector before entering valve V1 which regulates pressure. The flow rate is determined by the valve pressure and the dimensions of the pump tubing chosen and also the melt rate. After passing through valves and the debubbler, the meltwater is split into several lines that correspond to the analytes, dust and conductivity are also measured.

The **melthead** is located in the freezer and is used to continuously melt the ice core. It is made from gold coated material, making it chemically inert. This means it will not react with any of the impurities in the meltwater. The other purpose of the melthead is to separate the ice into the outermost, contaminated section of the ice core from the clean inner part used for chemical analysis. The melthead is heated with a temperature regulator. The temperature to which it is heated depends on several factors - how dense the ice is, the time resolution that is required and how many different analytes are being measured. A slower melt rate will achieve highest resolution. For the SubICE shallow cores, a temperature between 20-30^{o}C was used, the firn is porous and therefore quite sensitive to melting.

The meltwater passes through a **debubbler** which enables extraction of excess air from the sample. The sample water then passes through an automated valve system which selects between sample, standard solutions or blanks (Milli-Q: purified water) when no ice is being melted. The system is always pumping one of the three options in order to remove risk of contamination from air. These then proceed through the pumptubing to the individual detectors for analytical measurements to take place [Bigler et al. 2011].

In order to stabilize the meltspeed, a PTFE (Polytetrafluoroethylene) weight is placed at the top of each frame containing the ice core. This creates a constant vertical pressure. The meltspeed is therefore controlled by both the temperature of the melthead and how heavy the weight is. A draw-down wire sensor is attached to the weight and connected to an **optical encoder**. The encoder measures the meltspeed and this data can be used as a tool for obtaining the depth. However, as the ice melts, once the upper part of the frame is empty it must be replaced with the next frame in order to melt the ice continuously. During this short period, the meltspeed cannot be monitored and we get invalid values in the encoder data. This needs to be taken into account in the data processing and is described in further detail in Section 3.3.4.

A **conductivity meter** is used to measure Electrolytic conductivity which is the first measurement made as the sample passes through the system, followed by size and concentrations of insoluble particles, or "dust particles" using a **laser particle sensor**. The chemical analytical systems consist of both fluoresence spectrometers (for measurements of NH_4^+, H_2O_2, Ca^{2+}) and an **absorption spectroscoper** (for measurements of H^+ and Na^+). In the spectrometer, LEDs illuminate the sample at specific

wavelengths which excites the molecules of interest. Upon relaxation, the molecules will emit fluoresence which is detcted by the photon-multiplier sensors [Zens 2018].

After the melting process, the raw data from the analytical set-up needs to be calibrated in order to get the measurements in concentrations. Then the data is converted from real time onto a real depth scale. All processes were performed in Matlab and are described in detail below in Section 3.3.

3.3 Data processing

3.3.1 Standard calibrations

The CFA system measures the dust units of number of particles per millilitre and conductivity in units of μS. The remaining ionic species are measured using a combination of a fluoresence method and an absorption method. The signals produced are measured in units of photon counts and need to be converted into concentrations so the data can be more easily interpreted. In order to do this, it is necessary to first obtain known concentration of standards by running these through the system regularly throughout the melting process. Typically, a measuring campaign follows a daily structure as follows - morning standard run, a sample run of several metres of ice, a mid-day standard run, another sample run, followed by a final standard run at the end of the working day. For SubICE, there was approximately 3-5m of firn core per sample run. Depending on how much ice needs to be melted this routine is sometimes followed by more measurements, however the standard-sample-standard rule still follows. This helps to minimize calibration uncertainties that may be incurred from changes in the measurement conditions. The standard solutions are prepared in the lab using two pipettes with volumes 20 - 200 μL($\pm$ 0.2%-0.7%) and 100-1000 μL($\pm$ 0.2%-0.6%). They are made in accordance to the following table.

Multielement (MES)	μL	mL	ppb	Std no.
Stock solution			100000	
1st dilution	50	200	24.6	1
	100	200	49.3	2
	400	200	197.0	3
	2000	200	985.2	4
Peroxide	μL	mL	ppb	
Stock solution			300000000	
1st dilution	60	200	90000	
2nd dilution	100	75	120.0	5
	50	75	60.0	6
Acid HCl	μL	mL	uM	
Stock solution			100100	
1st dilution	600	60	1001	
2nd dilution	2400	120	20	7
	1200	120	10	8
Alkali NaOH	μL	mL	uM	
Stock solution			100100	
1st dilution	600	60	1001	Prepare as reqd
2nd dilution	2400	120	20	9*
	1200	120	10	9*

Tab. 2: Standard solutions as prepared for the SubICE campaign.

Using the standards of known concentration, a calibration coefficient is obtained for each standard file, for each ionic species. In general, the standard file that generates the most optimal for a particular sample run calibration will be either of the standard files closest in time to the sample run. It is likely that these will be best suited to that particular data set since if they are closest in time then it is unusual that any major changes will have been made to the system, such as integration time or reagent changes. Figure 25 in the Appendix shows how the calibration coefficients differ by reagent or change in integration time. There are often two standard runs, one before and one after the sample being melted. We choose whichever one gives a more reasonable output in concentrations. Sometimes, the coefficient is anomalous or standards were not run properly, in these types of cases there will be gaps in the coefficients. It is then required to just decide by testing the choice of calibration coefficients and judging by eye which looks the most suitable.

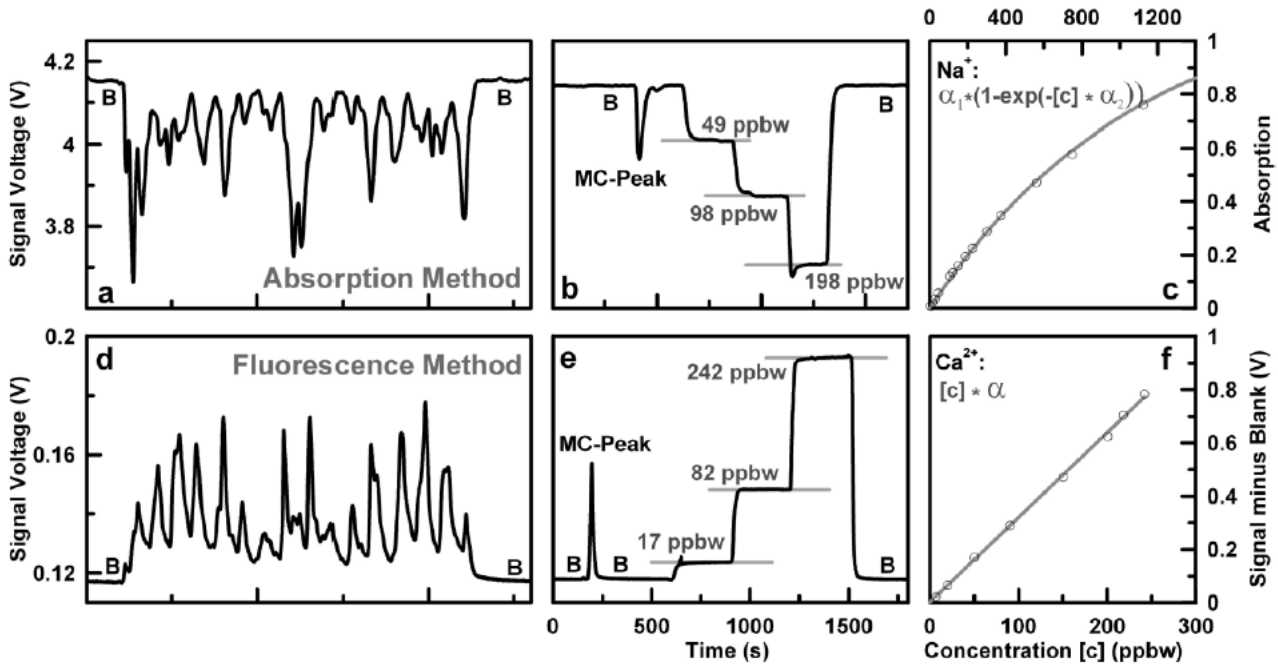

Fig. 9: Figure an example of a) an absorption method, b) standard run for an absorption method, c) exponention relationship between the concentration and absorption signal, d) a fluoresence method, e) standard run for a fluoresence method, f) linear relationship between concentration and the baseline removed signal.

In order to obtain the coefficients, the first step is to remove the baseline and then use Equation 1 to convert the photon counts into concentrations. This is done differently depending on which instrument was used. For the fluorescence method, the baseline is removed using the equation

$$F = I - I_0 = \epsilon \times c \times l \tag{1}$$

where c is concentration, l is length of the cell and epsilon is the molar extinction coefficient. The baseline, I_0, shown as B in Figure 9, is subtracted from the measured signal intensity, I to set the value of I_0 to a corresponding concentration of zero [Kaufmann et al. 2008]. The new signal, F, for each standard solution is regressed against the known concentrations. The slope of the linear fit, forced through zero, is the calibration coefficient, α, where $\alpha = \epsilon * l$. Rearranging the right hand side of the equation, the response signal can now be divided by the calibration to obtain the concentrations of analytes in the sample.

For measurements of acidity an absorption method is used which follows a log-linear relationship. The baseline of this signal is removed slightly differently, as shown in the equation

$$A = log(I/I_0) = \epsilon \times c \times l \tag{2}$$

Usually this would also imply a difference in the process obtaining the calibration coefficient, however since the data is in the linear range of the absorption counts-concentration relation, it was assumed that a simple division by the coefficient, α, could also be used here. The process above was done in this study using two different methods, manual and automated. Both of these were executed in Matlab and the two approaches are described in the following two subsections.

Manual method Consider the idealised example of a standard file shown in Figure 9, subfigure **e**. In this manual approach, first the standard data files are loaded. The code loops over each raw standard file and for each, there is a GUI implemented that enables the user to choose a start and end point for each standard within that file. A mean value is then calculated between these two points for each standard. This value is saved and used as input into a first order polynomial fit, alongside the concentrations used for each standard made. The code finally outputs a gradient corresponding to this fit, which is equal to the calibration coefficient value.

Automated method A code was written by myself, with guidance from my supervisors, in order to obtain the calibration coefficients more efficiently and quickly. The codes are slightly different depending on the core site in order to avoid unreliable data e.g. air in system. The automated method works in a similar way, however instead of choosing the boundaries that mark beginning and end of each standard with the GUI, the values were computed internally in the code. Conductivity values corresponding to a particular standard concentration tend to be similar within a small range for each run. Thus, the code scans across the data and uses some conductivity boundaries to test whether the conductivity values are in the right range for standard x, therefore estimating when each standard begins. In order to improve accuracy, the code also checks whether the "line" column (drawn from the raw data file) states whether the data lies where the standard x valve was initiated. Assuming that the code has chosen the right starting point, the code then computes a mean value in between some pre-defined time intervals (after the start point), for example $t_1 = startpoint + 60secs$; $t_2 = startpoint + 180secs$. The code computes a

mean based on the region chosen between time t_1 and t_2 and then saves this. Since there are different response times for each species the code is slightly different depending on which element is in question, it is split up into 3 sections: multi-element (Ca^{2+}, $NH4^{+}$), hydrogen peroxide (H_2O_2) and H^{+} ions. The chosen start and end values and means are then saved into an array and these values can be checked before proceeding. If all looks fine then the process continues as in the manual method, using the means photons and concentrations to find a linear fit.

3.3.2 Time delay

As mentioned in the previous section, the response time for the detector signals are different depending on the instrument. This is due to a variation in coil lengths or thicknesses of the pump tubing. In this CFA system, conductivity is measured first, so this is what is used as the reference. The delay time, ΔT then must be calculated for each other signal being detected, with respect to the conductivity. The data must all be on the same time scale in order to avoid offsets in depth when the concentrations are converted to a depth scale. Figure 10 displays an example of this difference in response time.

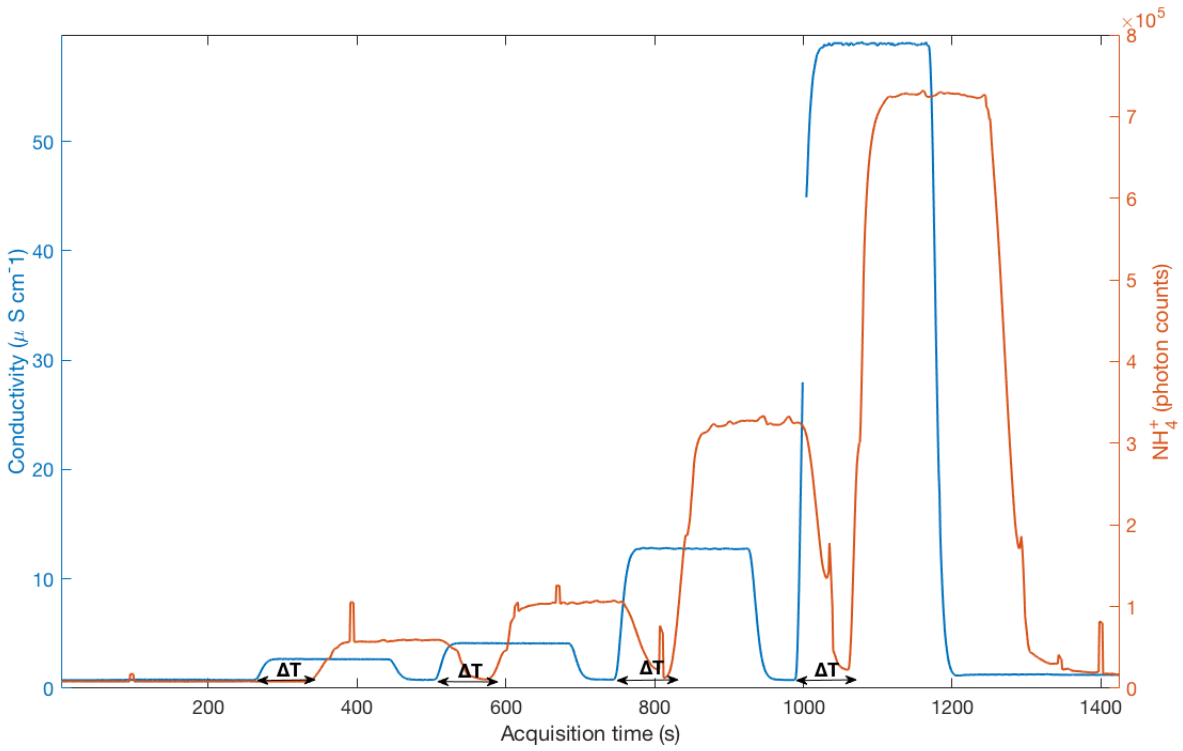

Fig. 10: Figure showing the response time delay between conductivity (blue) and $NH4^{+}$ during a standard file run in the Mertz Core melt run.

3.3.3 False trends and signal drift

Usually we are able to choose a constant baseline for a given standard run, accurate enough to remove from the whole data set. However, sometimes we get "drifting" of the data, which we use to describe a false trend in the data. This occurs most commonly in the pH but can also occur in the other signals. This process can be due to a number of things, including an ageing of reagents, but more commonly by wearing out of the pump tubing. The data set will then have a baseline before, vastly different to the baseline after the run and will require a time dependent baseline in order to calibrate correctly. In this case, the same procedure as discussed in 3.3.1 except a linearly changing baseline is chosen. This was achieved by adapting the GUI to account for a shifting baseline. Sometimes the data makes more of a step-jump in baseline levels rather than a gradual change. This can be accounted for by just removing the difference in baseline from whichever part of the data is out of place.

3.3.4 Depth scale

When the data has been converted from photons to concentrations, the next step is to have this data formatted onto a depth scale rather than in real time. The encoder is the key feature of the melt chamber that allows this to be done, it essentially measures the meltspeed, as described in the Encoder paragraph in Section 3.2.

Relative Depth The following equation can simply be used to obtain the relative depth.

$$Depth = \sum EncoderDifferential/EncoderValue \tag{3}$$

Before this can be done however, many things need to be adjusted within the data itself. The encoder has non-physical values when we have a frame change so the data needs to be interpolated across these regions of bad data to get a more reasonable range.

Real Depth Once everything is on relative depth scale, the way to get the data onto a real depth scale is by adding in all the breaks in the cores in all the right places. In this particular campaign, the firn cores were around 50-70cm in length and had between 0 up to 8 breaks. Breaks can occur internally when the drill pulls the core up from the borehole, during transportation or during handling in the

freezer. It is quite seldom the breaks are perfectly horizontal (w.r.t vertical core length), therefore any excess ice/firn must be shaved off so that it is always a flat surface being guided onto the melthead. There is also ice shaved off the top and the bottom in order to reduce contamination as much as possible. In most cases, the relative depth is offset from the real depth by several centimetres. It is important to add these lengths in at the correct places in order to ensure that if we want to produce the data on a real depth scale then it is as accurate as possible.

A code was written to add in the breaks and again, the general code is slightly altered for each core site to avoid complications with bad data. The code splits up the calibrated data into bag number, and has an input file containing information about on each bag and its corresponding number of breaks, break lengths and at what positions. The code loops over the bags, and within this, loops over the number of breaks and adds them in at the correct places, constantly updating the bag length before proceeding to the next bag. The code eventually outputs a new depth for the core, then adds NaNs to the data to distinguish between where there is real data and where there is no data.

3.3.5 Cleaning contamination

There are many sources of unreliable data which can arise during a melting campaign. The melting conditions tend to be worse when dealing with firn cores rather than ice cores. This is because the firn is so porous that the cores do not always fall so smoothly onto the melthead and can break easily causing air bubbles to get into the system. The final stage in data processing for this project was to clean the bad data from the calibrated, delay-adjusted, drift-corrected data, displayed as a function of depth. The noisy signals are filtered out - occurring from contamination on the edges and where the firn breaks have been touched with the knife. Also, sections where air got trapped or lines got blocked are manually removed.

3.3.6 Age scale (Mertz, Siple and Peter-First)

These firn cores are extremely difficult to date utilising a straight-forward annual layer counting method. In an ideal case, we would observe clear annual signals in proxies such as hydrogen peroxide (H_2O_2) or H^+, however, even the H_2O_2 signal in these regions does not contain as well defined annuals as we had hoped. We have therefore used a combination of techniques in order to attempt to date only Mertz, Siple and Peter-First. The three different approaches are described as follows

- Method one: find an area in the data where the H_2O_2 looks trustworthy, count the annuals in the chosen section, assume this can be extrapolated across the entire core;
- Method two: count the winter-winter peaks in the H_2O_2, using the melt layers as an aid;
- Method three: count the winter-winter peaks in the H_2O_2, using the $\delta^{18}O$ as an aid

The pros and cons of each method will be discussed in Section 5.

4 RESULTS

This chapter displays the processed results of the impurity analysis for the five SubICE firn cores melted in the CFA labratory at the University of Copenhagen. First, we present some useful tables followed by core-wise sections to display chemistry reconstruction, histograms of the data, statistical comparisons of the different sites and supplementary data where available.

4.1 Depth reconstruction

The table below displays the difference in measured length of each of the 5 cores. The field length refers to when the core was measured in the field after drilling, the freezer length is the length measured in the freezer when the cores are being prepared for the lab and the reconstructed length is the computed length using the information from the freezer logs and the encoder measurements.

Core	**Field length (m)**	**Freezer length (m)**	**Reconstructed length (m)**
Mertz 1	20.25 ± 0.15	20.13	20.21
Young Island	16.88 ± 0.14	16.89	17.17
Siple Island	24.14 ± 0.18	24.23	24.37
Peter-First Island	12.29 ± 0.09	12.27	12.26
Bouvet Island	13.84 ± 0.12	13.50	13.49

Tab. 3: Results of the depth scale reconstruction including error assessment for the SubICE cores.

There is an initial estimated uncertainty of ±0.5 cm per bag of ice in the field measurements. If there are disruptions during the melting process in the lab these will directly affect the encoder measurements.

4.2 Proxy deposition

The table below summarises the mean concentration values for the depth of the whole core for all the impurity measurements. The means are presented alongside the uncertainty given by ± the standard deviation. It is important to note that for some samples the data has been removed where it was thought to be unreliable e.g. destructed by means of diffusion. These values will be denoted with a '*' and the

data was trimmed as follows: Bouvet *all* impurities after 9.4m, Young H_2O_2 and H^+ after 11.0m, Mertz H_2O_2 after 13.5m. The table also shows the maximum values of the impurity data and a percentage melt layers in the core given by $\%melt = \frac{Totalmeltlayerthickness}{Reconstructeddepthofcore}$.

		Mertz	Young	Siple	Peter-First	Bouvet
$\mu \pm \sigma$	**Dust** [#mL^{-1}]	854.6±1134.0	4256±4252.0	450.9±616.1	1584.6±1298.0	6166.4±6803.0*
	Ca^{2+} [ppb]	8.9±9.0	71.7±55.9	12.8±14.7	15.9±15.0	5.3±6.1*
	NH_4^+ [ppb]	5.5±3.1	11.1±5.3	7.3±4.9	4.5±3.0	11.6±5.0*
	H_2O_2 [ppb]	7.7±8.2*	6.4±7.9*	29.8±23.9	21.3±25.1	7.7±5.6*
	H^+ [μM]	2.5±2.2	0.2±3.4*	1.5±2.1	0.2±1.6	0.4±1.0*
	Cond. [μScm^{-1}]	3.0±2.3	18.0±10.5	2.5±2.0	5.3±3.6	2.3±1.4*
Max. values	**Dust** [# mL^{-1}]	8085.0	21970.4	4977.8	6494.1	40532.1*
	Ca^{2+} [ppb]	58.9	248.8	80.5	85.4	44.4*
	NH_4^+ [ppb]	18.7	27.1	38.4	15.1	30.1*
	H_2O_2 [ppb]	68.8*	44.9*	131.0	135.8	17.1*
	H^+ [μM]	15.4	12.0*	14.0	5.9	3.5*
	Cond. [μScm^{-1}]	14.8	40.0	10.6	20.7	7.6*
% Melt		6.8	4.7	10.0	11.0	16.6

Tab. 4: Table of mean concentrations and their respective standard deviations, maximum concentration values and percentage melt layers for each SubICE core.

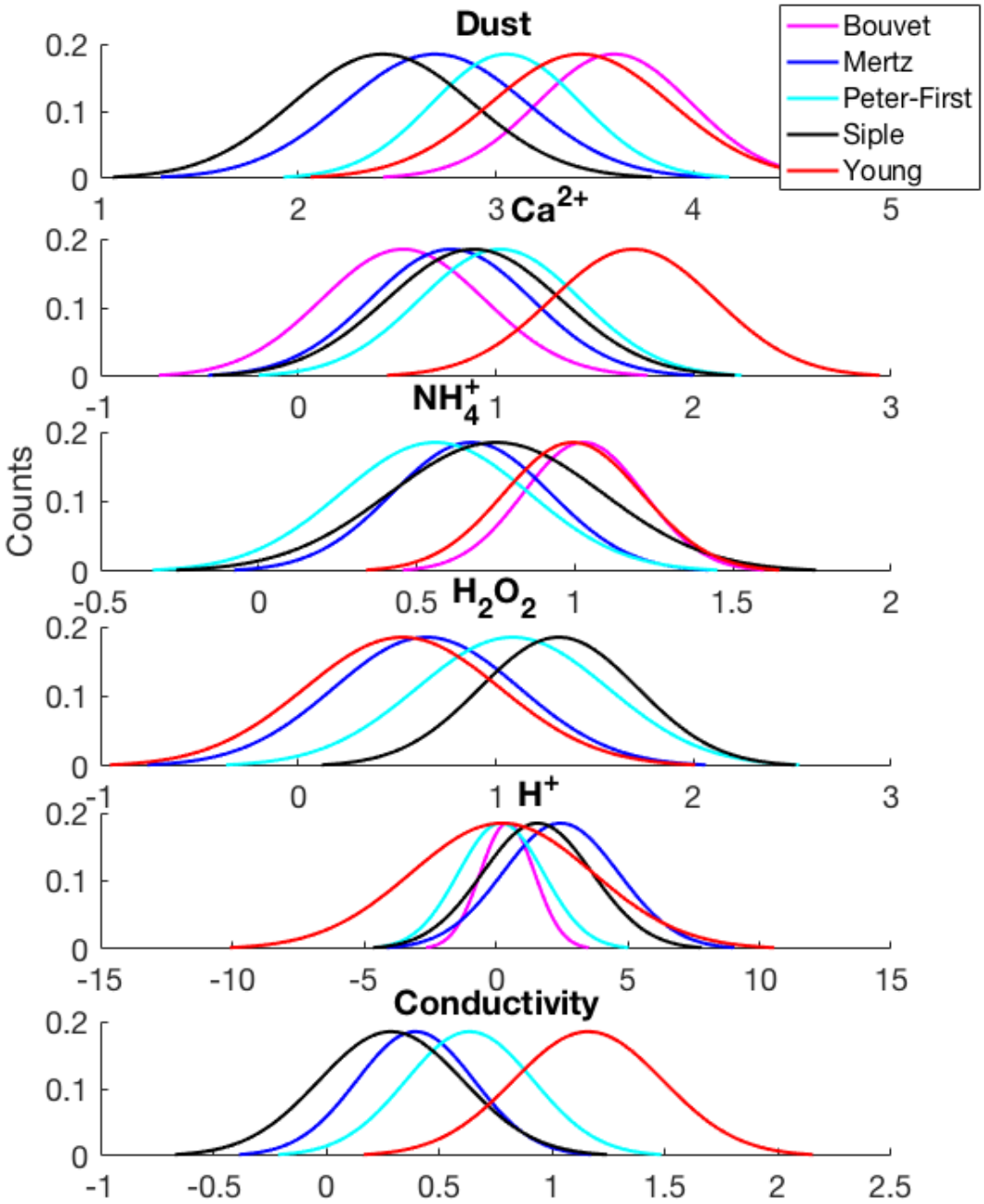

Fig. 11: Normalised site-wise comparisons of the lognormal distribution fits, displayed for each impurity.

We present an overview of the proxy deposition across the 5 firn cores. The impurity reconstruction is compared on a depth scale and some statistical analysis was performed on the data. Where data was available, other proxies are plotted in order to aid our suggestions. All the data is smoothed with smoothing factor based on an assumption of accumulation rate equal to $1myr^{-1}$ and with an aim to detect monthly features.

4.2.1 Mertz

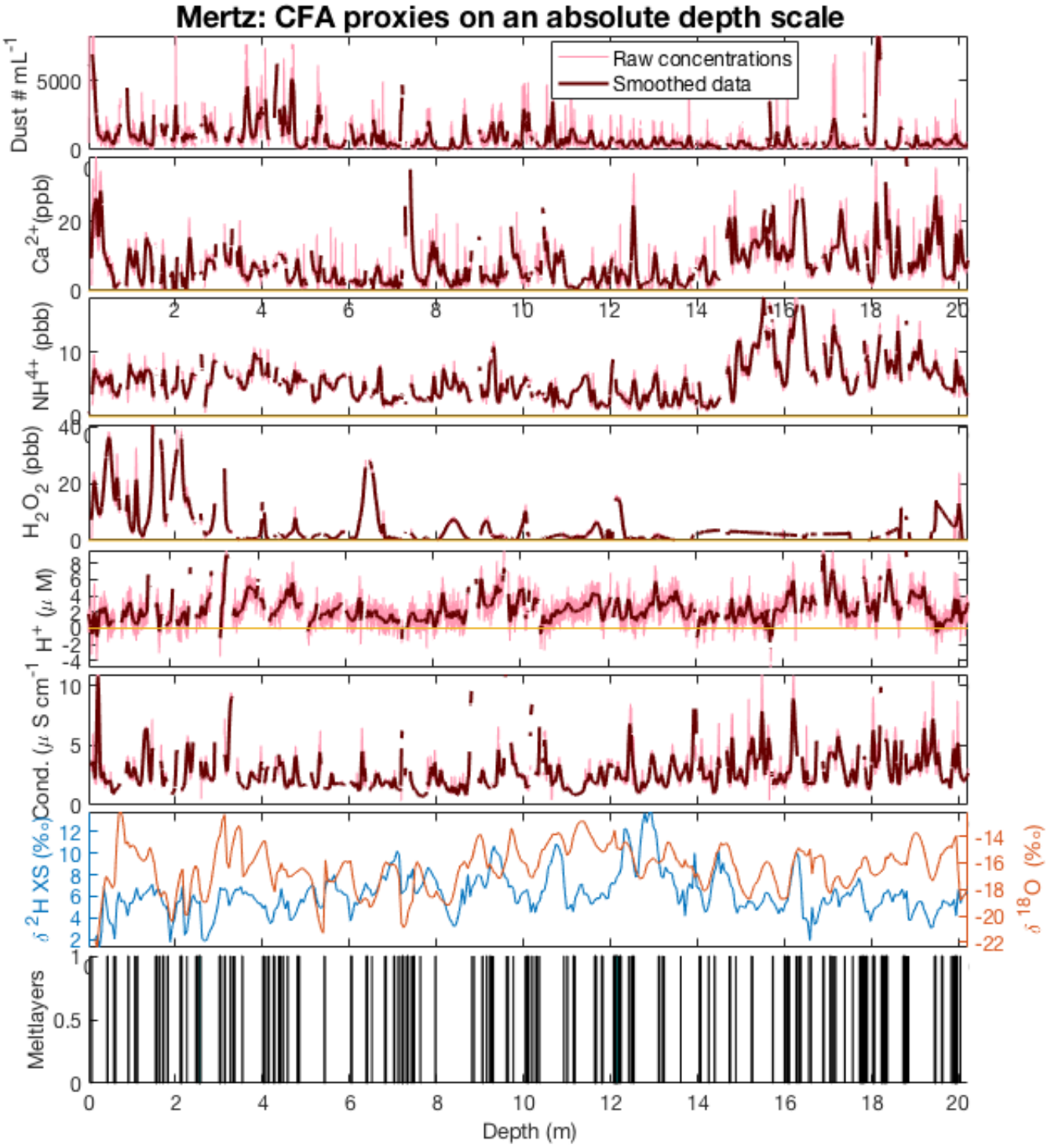

Fig. 12: Deposition of proxies on Mertz 1 as reconstructed by means of CFA analysis. Also displayed are stable water isotopes and melt layer thickness, both of which were measured by researchers at the British Antarctic Survey.

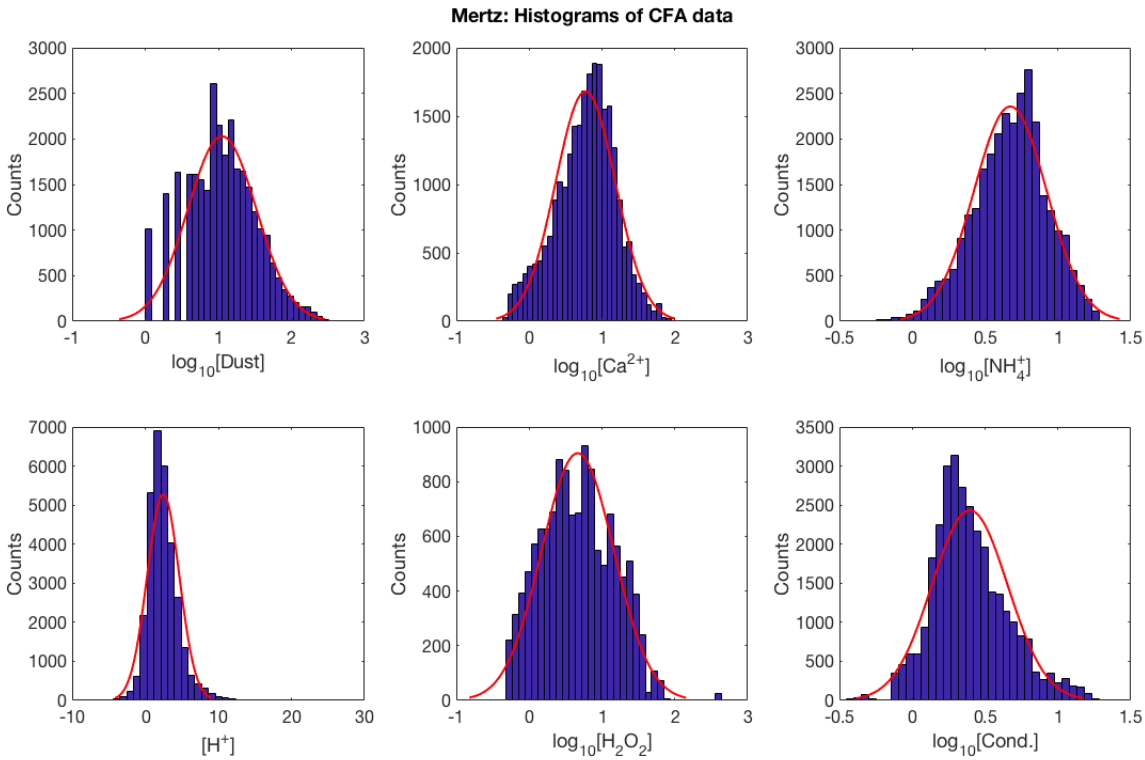

Fig. 13: Normalised histograms of the log-transformed impurity data for Mertz 1, fitted with a log-normal distribution.

4.2.2 Young

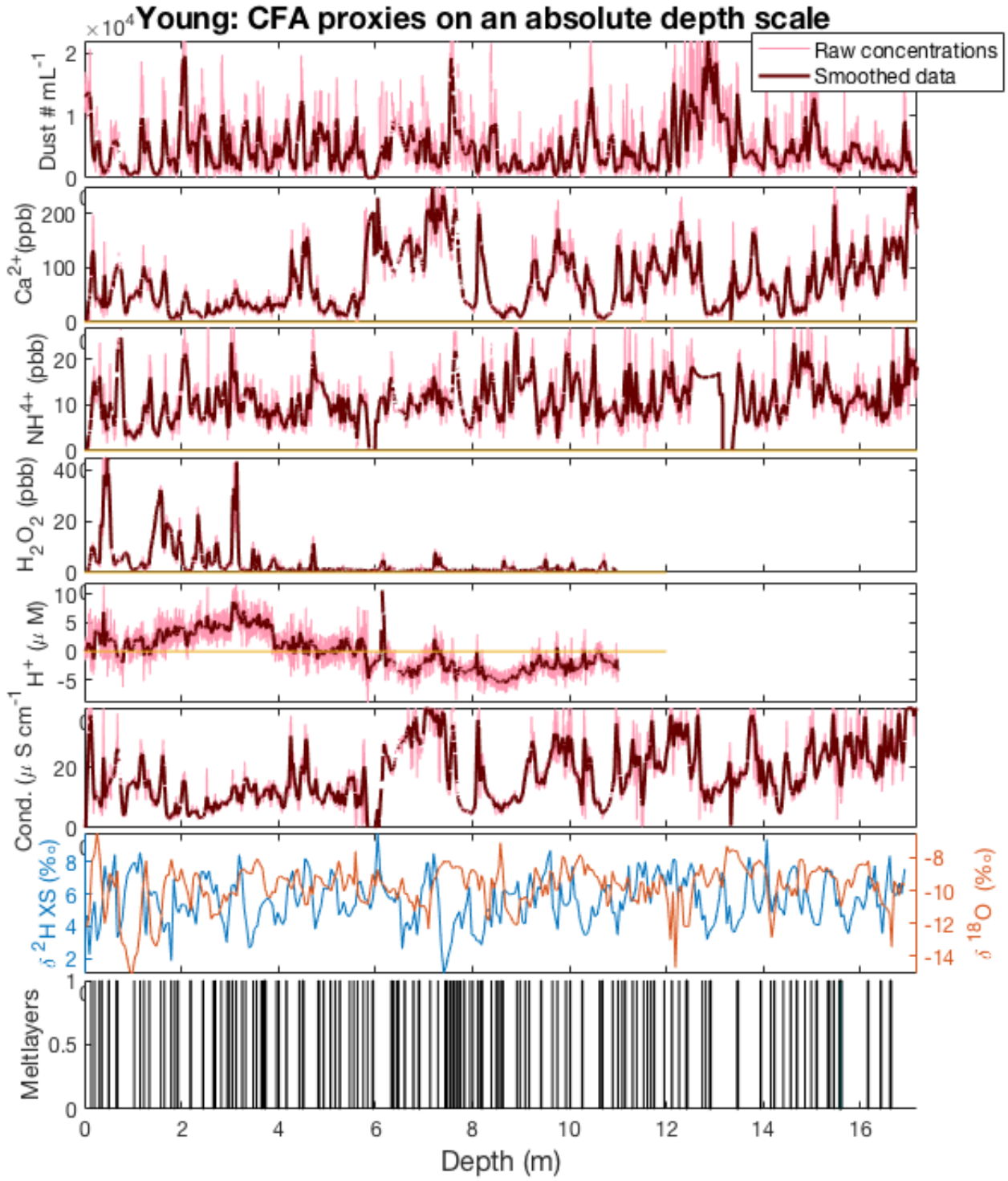

Fig. 14: Deposition of proxies on Young Island as reconstructed by means of CFA analysis. Also displayed are stable water isotopes and melt layer thickness, both of which were measured by researchers at the British Antarctic Survey.

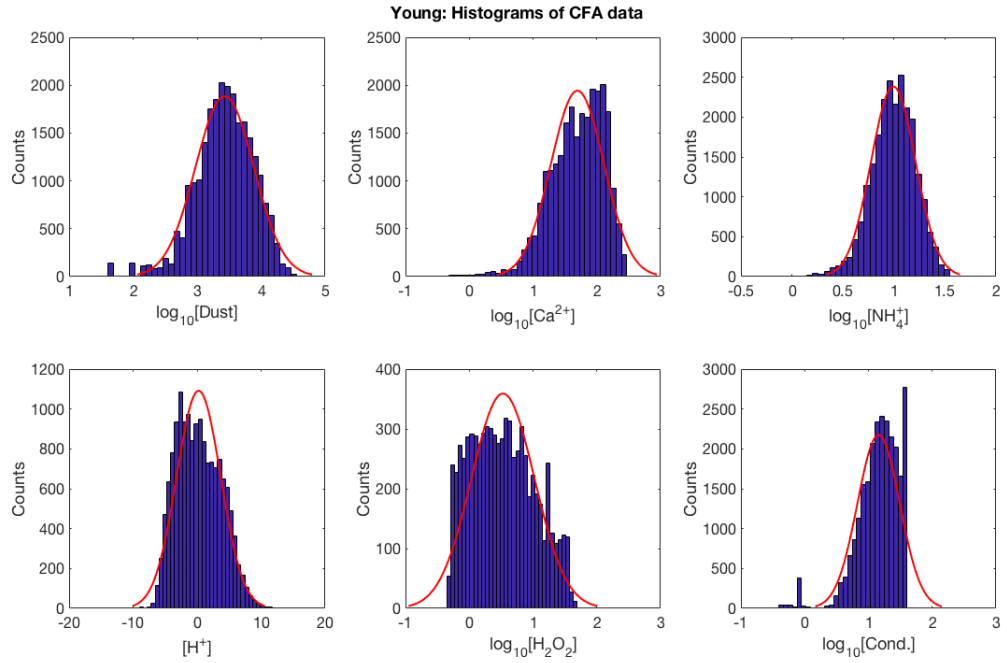

Fig. 15: Normalised histograms of the log-transformed impurity data for Young Island, fitted with a log-normal distribution.

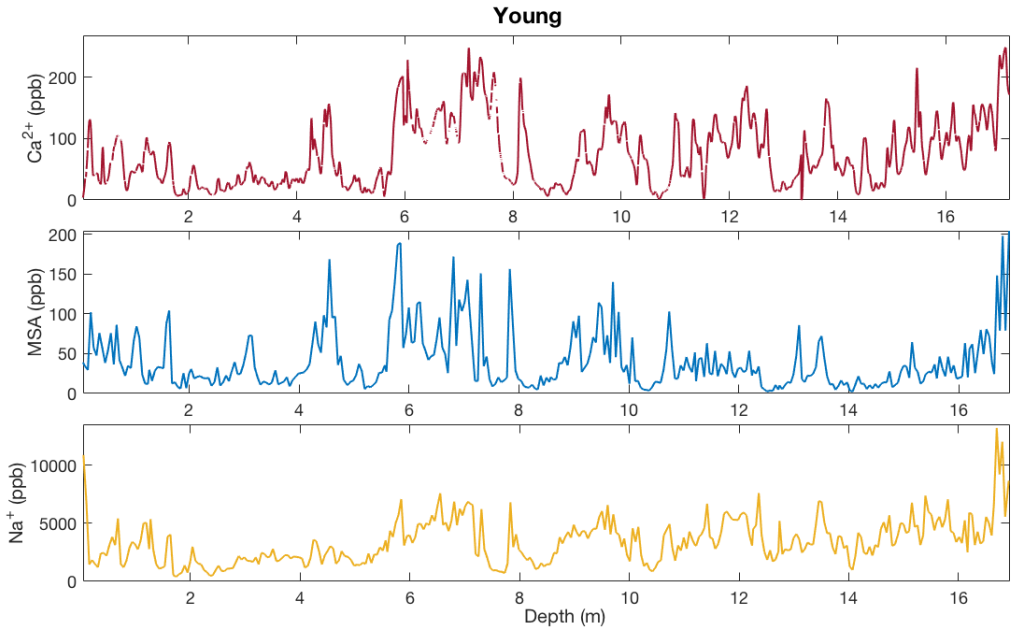

Fig. 16: Young Island MSA and Na^+ data reconstruction by means of discrete measurements undertaken by researchers at the British Antarctic Survey, presented alongside our Ca^{2+} CFA reconstruction.

4.2.3 Siple

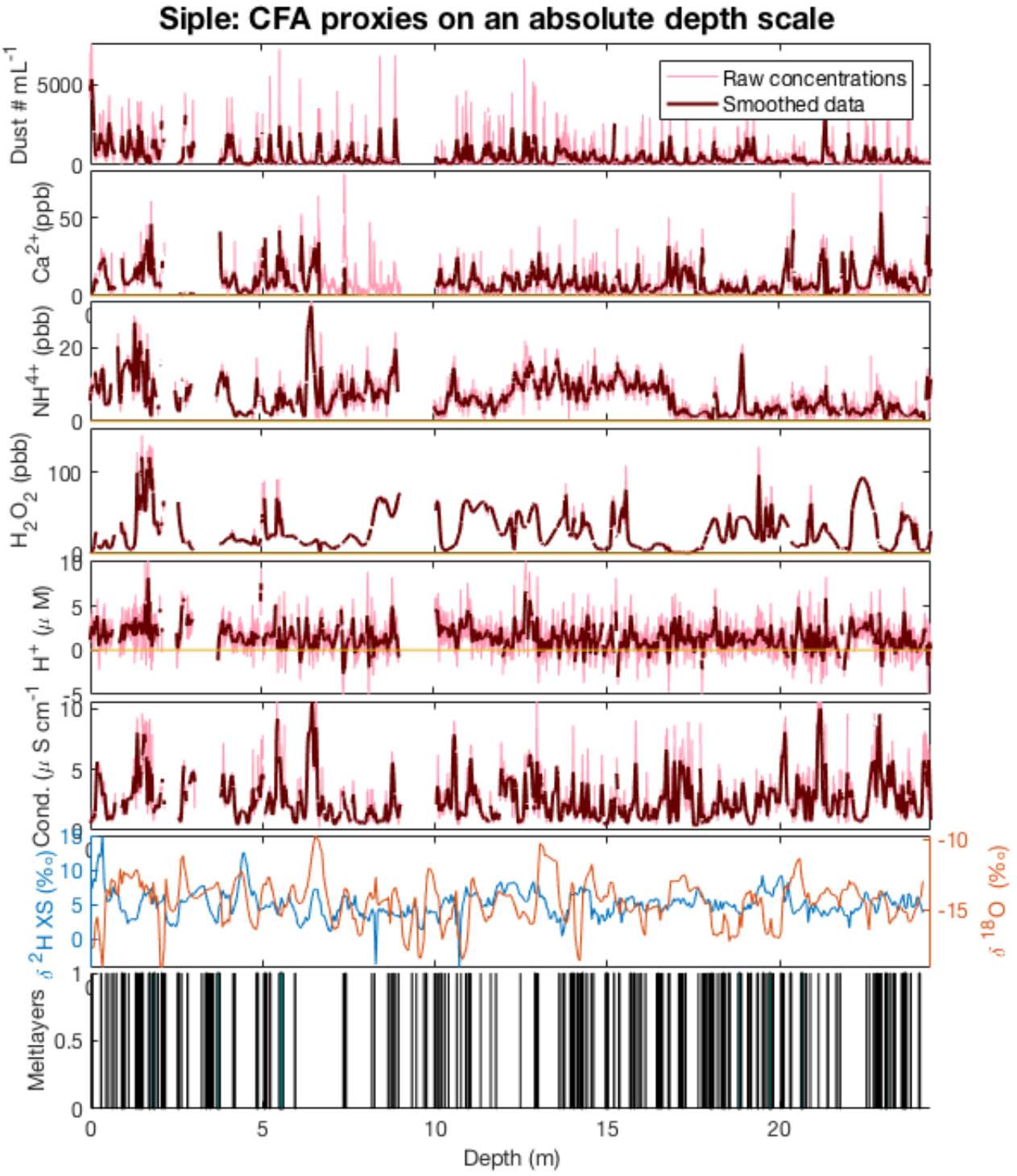

Fig. 17: Deposition of proxies on Siple Island as reconstructed by means of CFA analysis. Also displayed are stable water isotopes and melt layer thickness, both of which were measured by researchers at the British Antarctic Survey.

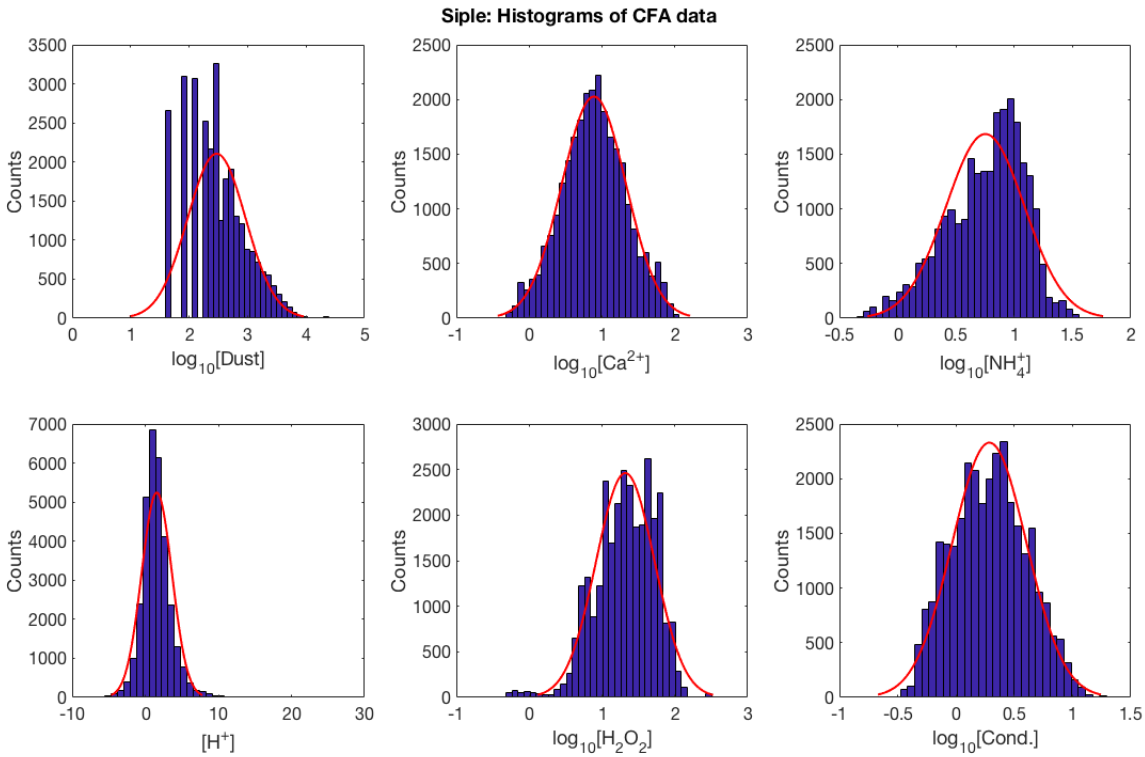

Fig. 18: Normalised histograms of the log-transformed impurity data for Siple Island, fitted with a log-normal distribution.

4.2.4 Peter-First

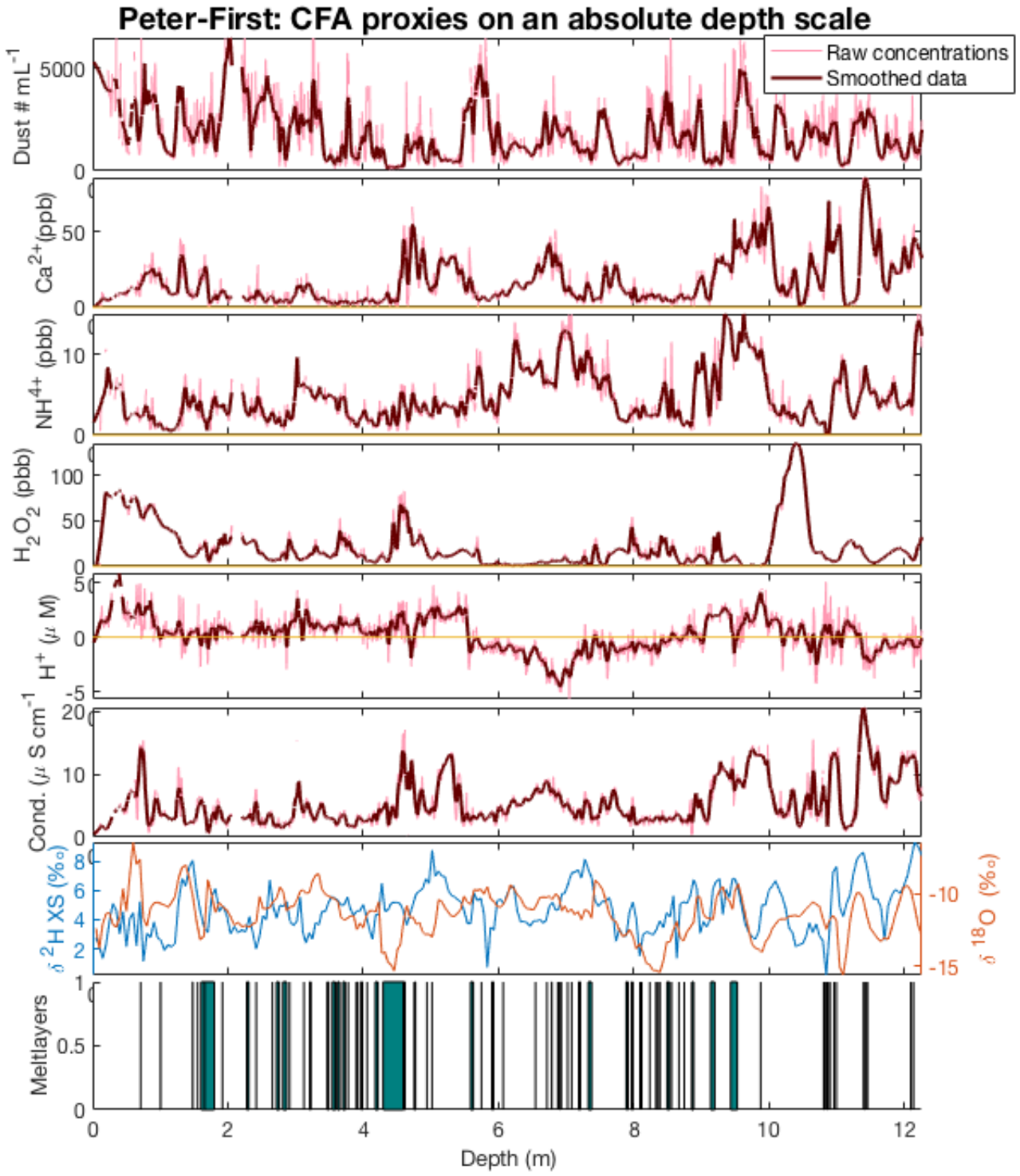

Fig. 19: Deposition of proxies on Peter-First Island as reconstructed by means of CFA analysis. Also displayed are stable water isotopes and melt layer thickness, both of which were measured by researchers at the British Antarctic Survey.

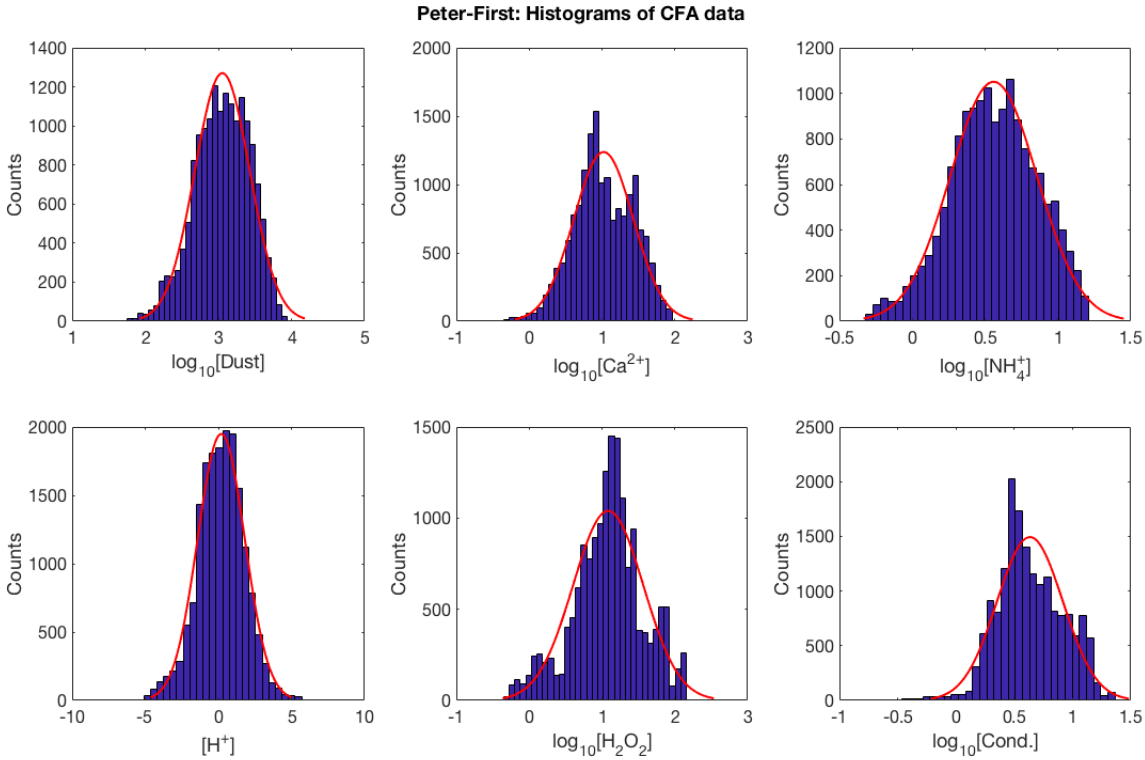

Fig. 20: Normalised histograms of the log-transformed impurity data for Peter-First Island, fitted with a log-normal distribution.

4.2.5 Bouvet

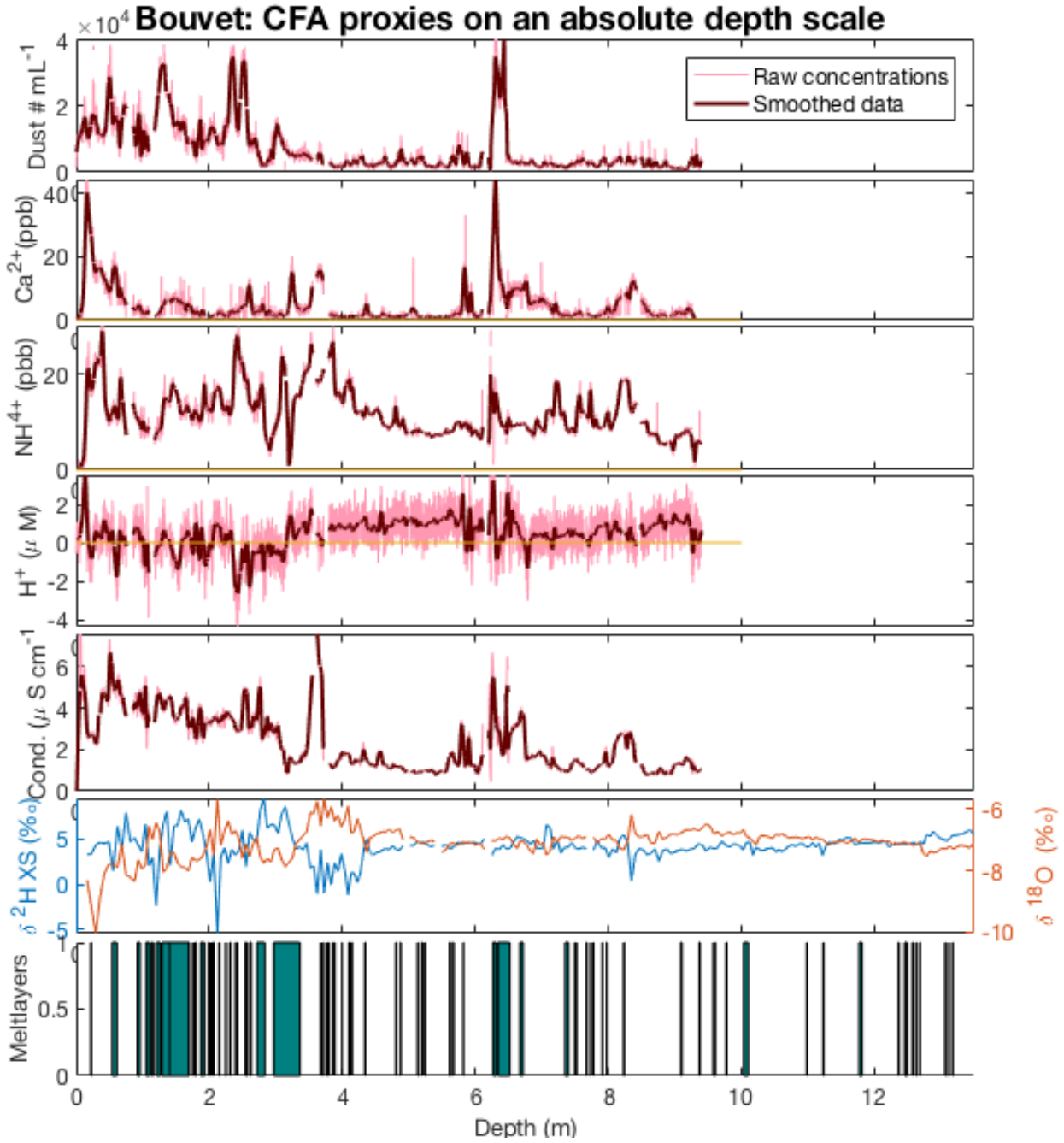

Fig. 21: Deposition of proxies on Bouvet Island as reconstructed by means of CFA analysis. Also displayed are stable water isotopes and melt layer thickness, both of which were measured by researchers at the British Antarctic Survey.

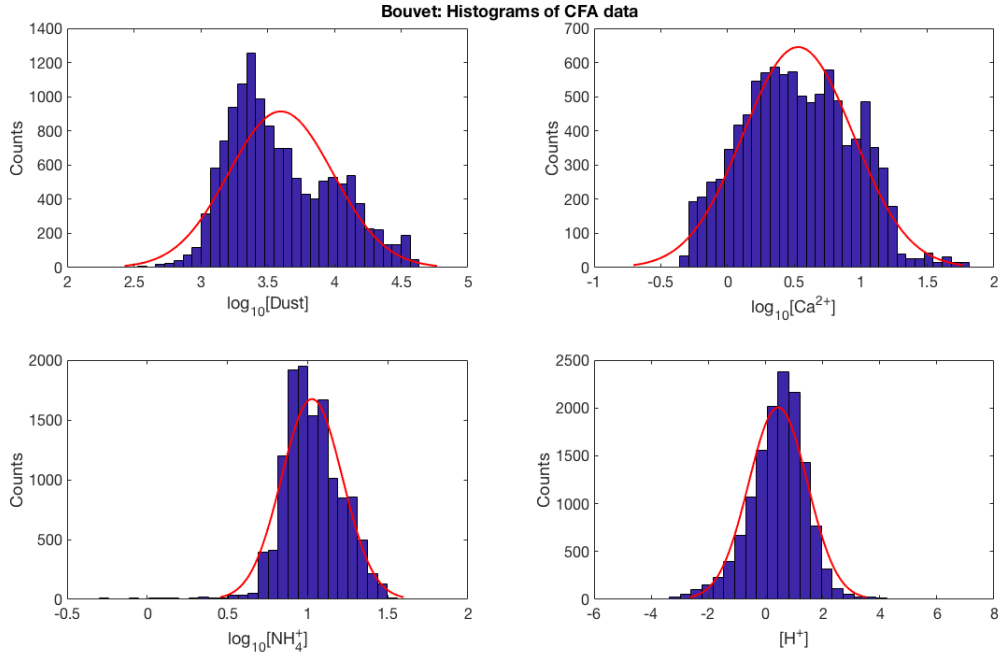

Fig. 22: Normalised histograms of the log-transformed impurity data for Bouvet Island, fitted with a log-normal distribution. Note that hydrogen peroxide and conductivity are discarded here due to non-physical histograms.

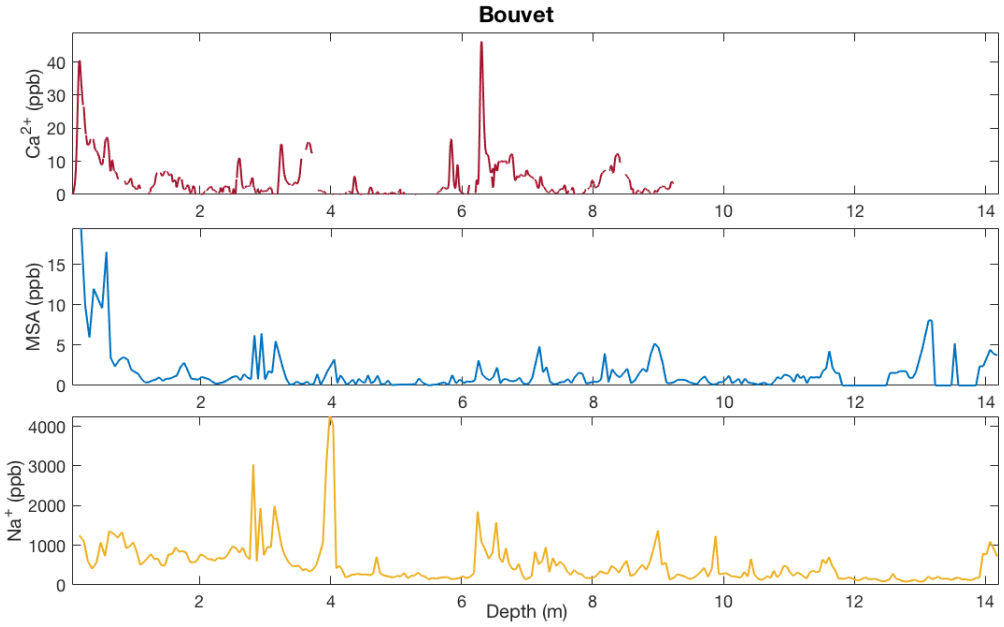

Fig. 23: Bouvet Island MSA and Na^+ data reconstruction by means of discrete measurements undertaken by researchers at the British Antarctic Survey, presented alongside our Ca^{2+} CFA reconstruction.

5 DISCUSSION

5.1 Depth reconstruction

Table 3 displays comparisons between field recorded lengths and encoder measured lengths. Mertz and Peter-First both differ only slightly and well within the uncertainty of their field-recorded length. Looking at Bouvet, the freezer length is smaller than the field length deviating outside the error boundaries. This indicates that Bouvet has suffered from transportation damage in cargo from the field to the lab in Copenhagen, losing somewhere between 0.22-0.46m. However, the reconstructed length is close to the freezer recorded length with only 1cm difference. Siple deviates slightly from the orignal recorded length, however, we argue that this is still reasonable if we allow for small mistakes to be made in the cutting logs. Young's reconstructed length is the most different from both the freezer length and the field length (+29cm approx.). Upon processing, when adding the breaks it was a much more complicated process for Young since the cutting logs had been produced in a different way to the other four firn cores. This meant that the code was not compatible with this format of adding the lost lengths. Therefore, a new cutting log was compiled based on the old one, whereby we calculated the values that would have been written had they followed the same structure as the other cores. This modification may have given rise to more errors in core length estimations and is likely to be the cause of this discrepancy. In summary, the reconstructed lengths coincide well within the boundaries for Mertz and Peter-First. Bouvet likely suffered loss in transit to Denmark. Siple's reconstructed length differs slightly from field length, however, the difference between freezer length and field length is minimal. This leads us to believe that the true original length was at the upper end of the error boundaries, therefore we do not see this difference as a major discrepancy. Young has quite a sizable deviation from field measurement which is probably due to accidental changes in core preparation methods.

5.2 Primary observations

5.2.0.1 Dust Insoluble dust particles are picked up from the continents and carried through the troposphere by winds, hence it is widely used as a proxy for global aridity and wind strength [Cuffey and Paterson 2010]. The first thing to note is in Table 4. The mean and maximum values of the dust concentration are highest in Bouvet, with a mean of approximately $6000\#mL^{-1}$ and maximum value of around $40{,}000\#mL^{-1}$. There is much lower dust depostion on Mertz and Siple, a factor of 10 less than that of Bouvet, Young or Peter-First. The high dust content could be due to the location of Bouvet, it would make sense that there is dust being transported from Southern African sources in addition to the usual Southern Hemisphere source, the Patagonia region. However, this would need further investigation to confirm, such as chemical composition analysis in order to distinguish between the two potential sources.

Another point of interest in Bouvet is in the dust signal. We can observe two distinct populations when looking at Figure 21. We suggest it could be related to the position and thicknesses of the melt layers as these align approximately. One explanation for the increase in dust amplitudes with the melt is that the hot summer temperatures could cause warm moist air to deposit an abundance of salts. However, if this was the case we would expect to see more peaks in either the Ca^{2+}, Na^{+} or both (see Figure 23 for Na^{+}). Therefore, we suspect it is something more to do with the way the dust behaves as the melting occurs. The melt layers in Bouvet are not only of highest percentage but also the layers are visibly much thicker than in the rest of the cores. If there is so much melt occuring then the meltwater can run off the glacier completely, leaving large amounts of dust particles behind. This in turn would result in high concentrations of dust per millilitre. This double population pattern can also be seen in the histograms. The histogram of the logarithmic dust signal in Figure 22 seems to have a bi-modal structure, whereas in Peter-First or Young they look much more like what we would expect from impurities in pure ice cores. Most airborne particles follow a lognormal distribution if being transported from a single source [*Aerosol Statistics Lognormal Distributions and dN/dlogDp*]. Therefore, this could further indicate two possible sources of dust: South American and South African regions.

As far as the other sites are concerned, there is not much to note regarding the dust itself, however it is worth mentioning that the higher dust concentrations in Bouvet, Young and Peter-First (all to the order of 10^3) could have an effect on H_2O_2 and/or H^{+} ions and will be further discussed in their

respective sections.

In summary, for the high bi-modal dust content in Bouvet we suggest 3 explanations: 1) Dry deposition of wind-transported dust from two different regions, 2) Hot summers with warm moist air depositing salts on the snow surface, 3) melt run-off leaving behind higher concentrations of dust. Whilst either of the three possibilities could be true, considering the presence of melt we hypothesise that the melt layers compromising the data is the most likely of the three.

5.2.0.2 Calcium The Calcium mean range is fairly similar for Mertz, Siple, Peter-First and Bouvet, with an exceptionally high mean recorded at Young Island. This goes for the maximum values also, see Table 4. In Figure 14 we can see that the calcium certainly correlates well with the conductivity rather than dust; suggesting this is a salt driven calcium signal observed in Young. The conductivity in Young will be further discussed in paragraph 5.2.0.6 and we will only focus on Ca^{2+} and its possible sources. In Figure 16 we can see that the Ca^{2+} is mostly in phase with the Na^{+} and possibly exhibits an even closer correlation with MSA. This supports a theory of a large marine contribution to the Ca^{2+} in this Sub-Antarctic core. This leaves us with an intriguing question - could this be fluctuations in sea ice extent as opposed to salts forming in bubbles on the ocean surface? We tried to test the mean ratio of Ca^{2+}/Na^{+} and check if it is closer to the ratio observed in the ocean vs. sea ice, however, neither stood out as a definite source. Therefore, this would require further investigation albeit such close agreement with MSA, a well-established sea ice proxy.

The second observation in the calcium was in the histograms, we notice a bi-modal distribution in Bouvet and Peter-First. As discussed in paragraph 5.2.0.1, in Bouvet this is likely due to heavy influence of melt. If it is not melt, this trend could be due to a combination of dust and sea salt contribution to the Ca^{2+} signal. Another alternative is that if the Ca^{2+} is dust driven, the signal could be originating from two different sources as suggested in paragraph 5.2.0.1 for Bouvet.

5.2.0.3 Ammonium Ammonium is a biospheric signal derived from low- and mid- latitude continents, usually emitted from soils, biota and fires but can also arise from algae in oceans and sea ice [Cuffey and Paterson 2010]. In Table 4 we can see that the mean concentrations of Bouvet and Young are almost double that of the other three cores. Bouvet and Young is where we see lowest max. values of hydrogen peroxide, especially Bouvet. Henceforth, if these are low accumulation sites then the

ammonium (and the dust) would be higher concentrations per mL of accumulation. In Bouvet, the high concentrations of ammonium could be due to the location. Bouvet is closer to the continents so higher signals being received in this region from land-based biotic sources in South America and South Africa. Another reason could be due to the high melt in Bouvet, if there is warm melt layers this could enhance the growth of bacteria. It could potentially indiciate presence of past cryoconite holes since these would produce a lot of black algae and croconite dust, hence also contributing to the high dust content. However, it is important to note that these are just speculations and would require further investigation.

5.2.0.4 Hydrogen peroxide Hydrogen peroxide is a highly established seasonal tracer in ice cores, with fluctuations due to enhanced photochemistry in the summer months. However, this method requires high accumulation rates, low dust deposition and a record with little melt to be valid [Legrand and Mayewski 1997]. The peroxide mean concentrations are fairly similar for Mertz, Young and Bouvet. Siple has the highest mean value at 29.8ppb followed by Peter-First with 21.3ppb. Since some of the data is not available for H_2O_2, it is more appropriate to compare maximum values here rather than means. Peter-First has the highest maximum at 135.8ppb and Siple 131.0ppb. Looking at the chemistry in Figure 19 this occurs during an alarmingly broad peak around 10-11m depth. There are some extremely thick melt layers in the upper half of the ice core which could explain why most of the hydrogen peroxide signal is destroyed. It could be that the melt layers are so severe that the signal has percolated downward to the deeper layers of the core causing an inteference with the true signal at depth. However, a more likely explanation is that it is a true signal since this corresponds to an area of little melt and of slightly higher quality annuals in the $\delta^{18}O$ (also very sensitive to melt). The high maximum levels of hydrogen peroxide in Siple and Peter-First could indicate higher accumulation in these sites in comparison to others.

The peroxide signal in Bouvet was not trustworthy throughout the whole core and therefore was discarded from the results entirely. It was written in the lab log book that the baseline was higher than the sample during the sample run. This dead signal could be due to either issues in the lab or the peroxide signal may have been totally destroyed. There are two possible causes for this damaged signal, although it is likely to be a combination of the two. It could have been destroyed due to the high percentage of melt layers - the highest of the 5 core sites - and with several extremely thick layers compared to cores

such as Mertz, Siple and Young. Such a high dust content on Bouvet could also explain the lack of high quality data in the hydrogen peroxide (H_2O_2). The signal amplitude is destroyed for almost the entire core (after 1m). Terrestrial oxidants can easily destruct hydrogen peroxide making the signal redundant for usage as an annual counting tool if the dust content is too high [Legrand and Mayewski 1997]. On the contrary, in Mertz and Siple the dust content is much lower, potentially allowing for less damaged peroxide signals and hence more identifiable annuals. Due to this high dust and melt inteference with the signal we hesitate to make any hypotheses regarding the accumulation in Bouvet.

Young also seems to have a reasonably weak peroxide signal. This site also has very high dust content. The data was removed after 11m since it looked unreliable. It is hard to spot any annuals here and therefore no attempt at an age estimate has been made here in this study for the Young core. Again, the peroxide signal here is too unreliable to comment on its implications of the accumulation.

Mertz and Siple have much more useful H_2O_2 profiles than the other cores. They both have the lowest percentage melt layers throughout and also the lowest dust desposition. These factors provide good conditions for storing the peroxide signals. Although Mertz seems to be undisrupted by dust or melt, the peroxide here does not stand out as particularly high in the mean or max. values. Therefore, we estimate a more modest accumulation rate for Mertz.

To summarise, firstly Bouvet's peroxide signal was likely to be destroyed due to a combination of high dust content and high presence of melt layers. In addition, it is likely that Young's weak signal is also a reflection of high dust content. Finally, Siple and Peter-First have the highest mean and maximum hydrogen peroxide signals. With higher accumulation rates, more layers form atop the snow surface storing the H_2O_2 signals beneath them. Contradictingly, if there was little accumulation the hydrogen peroxide would photolyse as the solar insolation penetrates through the upper layers, diminishing the signals. Hence, if we can assume that the signals are true and not affected by melt or dust, then these high peroxide signals would imply high accumulation for these sites.

5.2.0.5 Acidity In general, the data looks different to what we expect for acidity in pure ice. Ice cores such as NGRIP and RICE show that mean concentrations of H^+ tend to be in the range 1-5 $\mu eq/L$ [Kjær et al. 2016]. The means of Mertz and Siple look reasonable with respect to this expectation. However, Young, Peter-First and Bouvet look rather low in comparison and taking closer inspection at the chemistry for which, the data looks very unusual with high regions of negativity. The dust content

in these three cores was much higher than Mertz and Siple and we suspect this is not coincidental. It is likely that the large amounts of dust particles could have caused blockages in the absorption cell, inducing the subzero values that we see in Figures 21, 19 and 14. Therefore, the results of the H^+ ions at these sites is likely to be method dependent and hence unreliable.

Neither Mertz nor Siple show any indications of volcanic activity by eye-inspection. A reasonable test for volcanic eruptions would be to apply a 2 or 3 sigma test, where sigma is the standard deviation of the H^+ data [Miles 2011]. However, we did not carry this through since it is clear by eye that there are no alarming peaks in the data. Usually, we expect higher peaks in the H^+ in the presence of summer algae blooms, but when looking at Figure 12 and 17 there are no patterns of seasonality here either.

5.2.0.6 Conductivity The impurities in polar ice charecterize the core's electrical properties, hence, the conductivity is a quick indication of the impurity composition in ice cores [Cuffey and Paterson 2010]. Looking at table 4, the conductivity in most of the SubICE cores are within a similar range, with a mean of around 2.3±1.4 - 5.3±3.6 μScm^{-1}. The outlier here is Young Island, with mean conductivity of 18.0±10.5 μScm^{-1}. Several indications of Ca^{2+} driven conductivity lead us to believe that these higher levels are due to sea salts. Firstly, in figure 11 we can clearly see that the Young distributions are centred around the highest values for both conductivity and Ca^{2+}. Secondly, figure 15 shows similar behaviour in the log-transformed histograms of both conductivity and Ca^{2+} data, with the data skewed to the left in both. Finally, in the chemistry data itself in Figure 14 we can see that conductivity and Ca^{2+} have extremely similar profiles, with many peaks aligned in both signals. All these facts create a strong basis for sea salts dominating the conductivity signal in the region of Young.

5.3 Age-depth relation: Mertz, Siple and Peter-First

The three methods mentioned in Section 3.3.6 were trialed on Mertz and Siple, and one of the methods on Peter-First. The number of peaks obtained for each method is shown in the following table. Annual layer counting has been attempted at BAS using the stable water isotopes, however it is important to note that these are just preliminary results.

# of winter-winter peaks			
	Mertz	**Siple**	**Peter-First**
Method 1 (extrapolation)	33	40	15
Method 2 w/ melt	29	25	N/A
Method 3 w/ $\delta^{18}O$	33	28	N/A
BAS w/ isotopes	34*	28*	26*

Tab. 5: Table displaying the number of peaks counted in the three firn cores using the different methods. The '*' here denotes where an extra layer was counted that was not a full year (2017).

As for Mertz, the three methods used seem to agree fairly well with each other and with BAS' estimate. An example of the process is shown in Figure 26 for Method 2 and Figure 27 for Method 3, both in the Appendix. Siple agree fairly well except for the extrapolation method. Our counting of annuals in Peter-First does not agree well with BAS' interpretation. The range of no. of peaks counted in the data corresponds to an age estimate of the oldest layer equal to 1982-1987 for Mertz, 1977-1991 for Siple and 1990-2001 for Peter-First. The corresponding estimates of accumulation, based on a mean firn density of $500kgm^{-3}$, are as follows: Mertz 0.3m w.eq., agreeing with BAS' prediction of 0.32m w.eq. Siple 0.3-0.4m w.eq. and Peter-First 0.4m w.eq. It is difficult to say whether or not these seem reasonable, but they are not in agreement with how the maximum peroxide values compare with each other. There is records from Siple station stating that accumulation in this region is 0.5m w.eq. annually, since Siple Island is a coastal region, in a more moist area, closer to the precipitation source we would expect that accumulation would be higher than that of Siple station. Hence, for these two reasons, we are not convinced that these values are close to the true accumulation rates for these islands.

Each method has its advantages and disadvantages. Method 1 assumes a small section of hydrogen peroxide to be reliable and extrapolates across the core. This is helpful in the sense that we can apply it even when there only a few visible annuals, however, it is safe to say that these sites vary in accumulation year to year. Therefore, we argue that it is not valid to assume that the layer thickness is similar each year for each individual core site, especially where there is high presence of melt. Method 2 uses the melt layers to help identify where there are summer peaks. The problem with this is that there seems to be melt layers throughout the core, not always coinciding with summer maxima. This could be due to

diffusion of signals caused by the melt layers themselves. Method 3 uses the the stable water isotopes in order to help identify synchronous peaks between the peroxide and $\delta^{18}O$. Much like the peroxide itself, water molecules in the firn and pore spaces can exchange with the overlying atmosphere [Cuffey and Paterson 2010]. Therefore, this gives rise to disagreements between dating of cores using isotopes and peroxide; particularly in areas of low accumulation i.e. burial is slow or coastal regions susceptible to strong winds causing snow removal. In summary, it is often useful to combine dating methods in order to get a more reliable estimate. There is not enough evidence shown in this brief age-depth analysis to accurately date the core.

6 CONCLUSION

This project uses a high-resolution continous flow analysis (CFA) method to reconstruct electrolytic conductivity and impurity measurements for five Sub-Antarctic shallow firn cores recovered between December 2016 - March 2017. The five cores - Mertz 1, Siple Island, Young Island, Peter-First Island and Bouvet Island - constitute the Sub-Antarctic Ice Coring Expedition (SubICE), part of the internaitonal Atlantic Circumnavigation Expedition. The CFA technique in this SubICE campaign used a combination of fluorescence and absorbance spectroscopy to detect Ca^{2+}, NH_4^+, H_2O_2 and H^+. The system also uses an Abakus for continuous laser particle counting and measures electrolytic conductivity. The SubICE campaign took place in June 2018 at The University of Copenhagen. The aim of the project was to convert the impurity data to concentrations, followed by reconstruction of the cores' depth scale and where possible, estimate an age for the ice.

The statistics tells us that the data is extremely widely distributed. In many cases the standard deviation is larger than the mean concentrations. A possible cause is that the data is lacking in zeros, creating a positive skewness upon the data. However, this could also be interpreted as the lognormal distribution being an incorrect fit for some of the data, which would also epxlain the offsets in some of the histogram fits. This should be investigated more deeply as it does not agree with our current understanding of aerosol deposition behaviour e.g lognormal distribution of proxies.

We find that Bouvet experiences bi-modal behaviour in the dust and calcium signals and speculate that dry deposited dust in this region either has multiple sources or the signal is heavily influenced by thick meltlayers. Young Island displays high conductivity levels and calcium signals, implying that sea salts may dominate here. Phase alignments with sodium help support this, and correlations with MSA suggest it could be due to changes in sea ice extent rather than a marine source. Mertz and Siple exhibit some areas of seasonality in the hydrogen peroxide and we estimate an age-depth relation for these cores. Siple and Peter-First contain the highest concentration maximums of peroxide, indicating these are regions of high accumulation relative to the other cores. Generally, these cores are heavily affected by melt and high dust deposition. In essence, the remote locations of these islands and strong winds inhibit simple interpretations of proxies. However, they provide us with a wealth of information

regarding recent climatic changes in the Southern Hemisphere. Hence, it is imperative that we further investigate some of the hypotheses that are speculated in this project.

Several methods were used to estimate the age of Mertz and Siple, including one method for Peter-First. Each approach gives slightly different results and we are therefore unable to deduce which method is the most trustworthy since the data is so complex. Given more time, an attempt at a more accurate dating method would have been constructed. This study was unable to make an accurate dating of the cores, attributable to disruptions in stratigraphy and diffusion of analytes. An alternative method that was discussed was to perform a spectral analysis on each of the impurity records. If the power spectra resulted in the same dominant wavelength for each impurity (corresponding to annual layer thickness), that would allow us to distinguish between annual layers more easily. Complications with missing data inhibited us from conducting this analysis with ease, therefore we were unable to conduct this analysis due to time constraints. This would be something worth investigating, however, success is not guaranteed. Another significant resource would be the calibrated processed Na^+ CFA data for Mertz, Siple and Peter-First. BAS constructed Ion Chromotography for Na^+ on Bouvet and Young only. This was a useful tool in identifying whether Calcium coincided with sea salts, hence, would also be advantageous for the other three cores.

Overall, these areas of the Sub-Antarctic are wildly understudied. There are no published studies for most of these cores, all except Bouvet, therefore proving no means for comparisons or validations of our scientific outcomes. To this end, combined with the sheer complexity of these cores, we do not conclude any theories with high confidence levels. However, this study is an extensive initial insight into these crucial areas for Southern Hemisphere climate interpretation, and provides direction for future studies.

7 ACKNOWLEDGEMENTS

Firstly, I would like to thank my dedicated supervisors, Helle Astrid Kjær and Paul Travis Vallelonga, for offering me continued support throughout this exciting project. Thank you for your advice and thorough guidance, often within a moments notice! I would also like to thank Anders Svensson for always being available in the event that I need the extra support.

Thanks to the Centre for Ice and Climate, the British Antarctic Survey and members of the SubICE project for giving me the opportunity to conduct this fascinating thesis and introducing me to the world of ice core research. I thoroughly enjoyed my time spent in the lab and the ice core freezer getting to know the process involved in this expert area of climate research.

Thank you to my amazing mum and partner for extensive proof-reading and copious amounts of support and praise. And of course, to all my course friends that I've met along the way, particularly Mathias Skov Jensen and Janani Venkatesh, who have stuck by my side throughout this Masters with their kind support and generous help over the past two years. I express my appreciation and considerable gratitude to all mentioned or involved in the above.

8 BIBLIOGRAPHY

References

(1) Abram, N. J.; Mulvaney, R.; Wolff, E. W.; Mudelsee, M. *Journal of Geophysical Research: Atmospheres* **2007**, *112*.

(2) Albert, M. R. *Annals of Glaciology* **2002**, *35*.

(3) Berger, A. *Reviews of Geophysics* **1988**, *26*.

(4) Bigler, M.; Svensson, A.; Kettner, E.; Vallelonga, P.; Nielsen, M.; Steffensen, J. *Environmental science and technology* **2011**, *45*.

(5) Boyd, P. et al. *Nature* **2000**, *407*.

(6) Bradley, R. S., *Paleoclimatology: Reconstructing Climates of the Quaternary*, 3rd; Elsevier: 1999.

(7) CFA Impurity Measurements., `http://www.iceandclimate.nbi.ku.dk/research/drill_analysing/cutting_and_analysing_ice_cores/cfa/`.

(8) Cuffey, K. M.; Paterson, W. S. B., *The Physics of Glaciers*, 4th Edition; Elsevier: 2010.

(9) Curran, M. A. J.; van Ommen, T. D.; Morgan, V. I.; Phillips, K. L.; Palmer, A. S. *Science* **2003**, *302*.

(10) Dansgaard, W.; Johnsen, S. J. *Journal of Glaciology* **1969**, *8*.

(11) Fischer, H.; Siggaard-Andersen, M.-L.; Ruth, U.; Räthlisberger, R.; Wolff, E. *Reviews of Geophysics* **2007**, *45*.

(12) Hamilton, G. S.; Blue spikes, V.; Stearns, L. A. *Annals of Glaciology* **2005**, *41*.

(13) Herron, S.; Hoar; Langway, C. C. *Journal of Glaciology* **1979**, *23*.

(14) Joel Pedro, B. M.; Gaticúa, G. SubICE Leg 2 Report.

(15) Jouzel, J. et al. *Science* **2007**, *317*.

(16) Kaufmann, P. R.; Federer, U.; Hutterli, M. A.; Bigler, M.; SchÃŒpbach, S.; Ruth, U.; Schmitt, J.; Stocker, T. F. *Environmental Science & Technology* **2008**, *42*.

(17) King, A. C. F.; Thomas, E. R.; Pedro, J. B.; Markle, B.; Potocki, M.; Jackson, S. L. e. a. *Geophysical Research Letters* **2019**, *46*.

(18) Kjær, H. A. Continuous Chemistry in Ice Cores: Phosphorus, pH and the Photolysis of Humic Like Substances, Ph.D. Thesis, The Niels Bohr Institute of Science, University of Copenhagen, 2014.

(19) Kjær, H. A.; Vallelonga, P.; Svensson, A.; Elleskov L. Kristensen, M.; Tibuleac, C.; Winstrup, M.; Kipfstuhl, S. *Environmental Science & Technology* **2016**, *50*.

(20) Lamarque, J.-F.; McConnell, J. R.; Shindell, D. T.; Orlando, J. J.; Tyndall, G. S. *Geophysical Research Letters* **2011**, *38*.

(21) Legrand, M.; Ducroz, F.; Wagenbach, D.; Mulvaney, R.; Hall, J. *Journal of Geophysical Research: Atmospheres* **1998**, *103*.

(22) Legrand, M.; Mayewski, P. *Reviews of Geophysics* **1997**, *35*.

(23) Meese, D. A.; Gow, A. J.; Alley, R. B.; Zielinski, G. A.; Grootes, P. M.; Ram, M.; Taylor, K. C.; Mayewski, P. A.; Bolzan, J. F. *Journal of Geophysical Research: Oceans* **1997**, *102*.

(24) Miles, G. Detection and Effects of Volcanic Sulphur in the Stratosphere., Ph.D. Thesis, University of Oxford, 2011.

(25) NCAR UCAR Climate Data Guide., `https://climatedataguide.ucar.edu/`, 2019.

(26) NEEM community members et al. *Nature* **2013**, *493*.

(27) PAGES2k Consortium et al. *Scientific Data* **2017**, *4*.

(28) Rasmussen, S. O. et al. *Journal of Geophysical Research: Atmospheres* **2006**, *111*.

(29) Rignot, E.; Jacobs, S.; Mouginot, J.; Scheuchl, B. *Science (New York, N.Y.)* **2013**, *341*.

(30) Ruddiman, W. F., *Earth's Climate: Past and Future*, 3rd Edition; Macmillan Education: 2014.

(31) Schüpbach, S.; Federer, U.; Kaufmann, P.; Albani, S.; Barbante, C.; Stocker, T. F.; Fischer, H. **2013**.

(32) Solomon, S.; Plattner, G.-K.; Knutti, R.; Friedlingstein, P. *Proceedings of the National Academy of Sciences* **2009**, *106*.

(33) SPI ACE Expedition., `https://spi-ace-expedition.ch/bouvet-the-last-stop/`, 2016-2019.

(34) Stocker, T.; Qin, D.; Plattner, G.-K.; Tignor, M.; Allen, S.; Boschung, J.; Nauels, A.; Xia, Y.; Bex, V.; Midgley, P., *IPCC, 2013: Climate Change 2013: The Physical Science Basis. Contribution of Working Group I to the Fifth Assessment Report of the Intergovernmental Panel on Climate Change*; Cambridge University Press: 2013.

(35) SubICE., `https://www.bas.ac.uk/project/subice-sub-antarctic-ice-coring-expedition/`, 2016-2019.

(36) Sutton, M. A.; Asman, W. A. H.; Schžring, J. K. *Tellus B: Chemical and Physical Meteorology* **1994**, *46*.

(37) Svensson, A.; Andersen, K. K.; Bigler, M.; Clausen, H. B.; Dahl-Jensen, D.; Davies, S. M.; Johnsen, S. J.; Muscheler, R.; Parrenin, F.; Rasmussen, S. O.; Röthlisberger, R.; Seierstad, I.; Steffensen, J. P.; Vinther, B. M. *Climate of the Past* **2008**, *4*.

(38) Svensson, A. In *Encyclopedia of Scientific Dating Methods*, Rink, W. J., Thompson, J., Eds.; Springer Netherlands: Dordrecht, 2013, p 341.

(39) Thornes, J. E. *International Journal of Climatology* **2002**, *22*.

(40) Wagenbach, D.; Ducroz, F.; Mulvaney, R.; Keck, L.; Minikin, A.; Legrand, M.; Hall, J. S.; Wolff, E. W. *Journal of Geophysical Research: Atmospheres* **1998**, *103*.

(41) Wolff, E. W.; Rankin, A. M.; Rathlisberger, R. *Geophysical Research Letters* **2003**, *30*.

(42) Zens, P. Aerosol Input and Snow Accumulation Rates on Northern Greenland Ice Sheet: Reconstructed by means of Continous Flow Analysis (CFA) of 6 shallow firn cores., MA thesis, University of Copenahgen, 2018.

A APPENDIX

Fig. 24: Map of the SubACE leg 2 route (highlighted in red). Most of the SubICE cores were drilled during leg 2, all except Bouvet Island which was drilled in the 3rd leg of the expedition (grey). The Islands chosen for SubICE are highlighted in green, going anti-clockwise is Bouvet Island, Peter 1st Island, Mt Siple (Siple Island), Balleny Islands (Young Island) and Mertz Glacier.

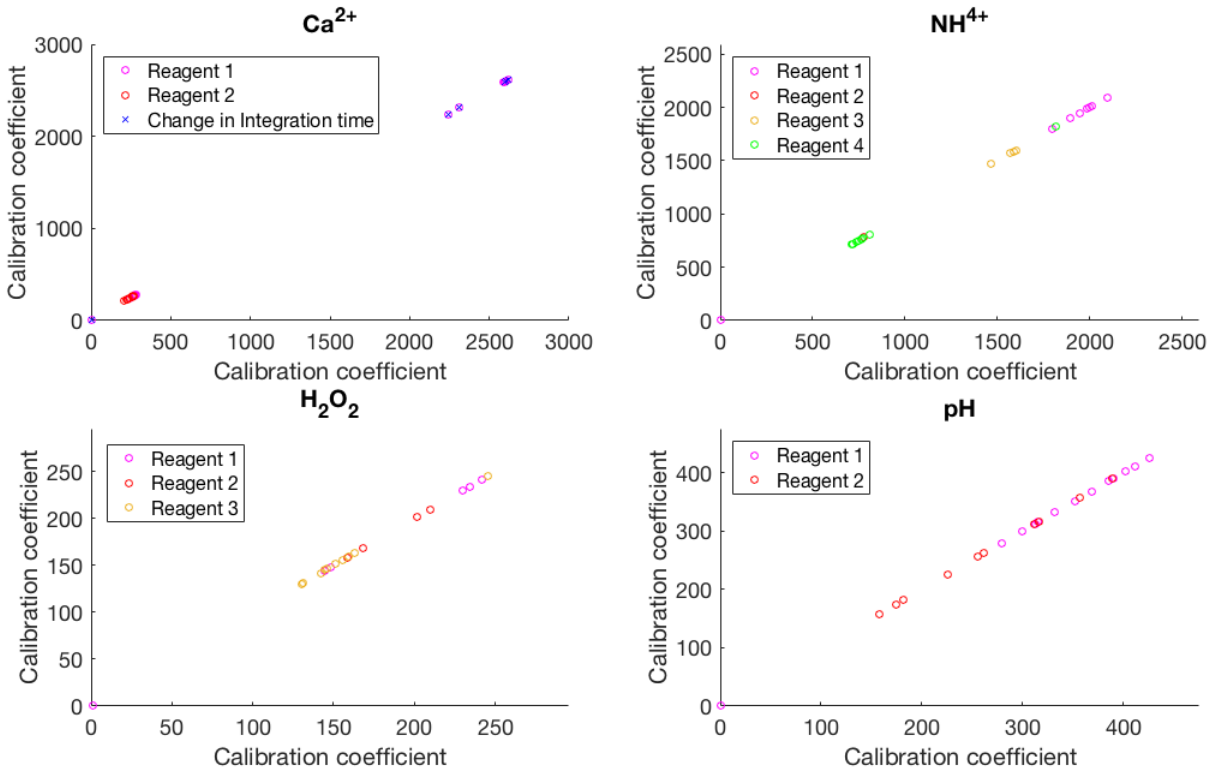

Fig. 25: Figure displaying the calibration coefficients for the chemical impurities. Colour indicates differences in reagent and in the case of calcium, an 'x' denotes change in intergration time.

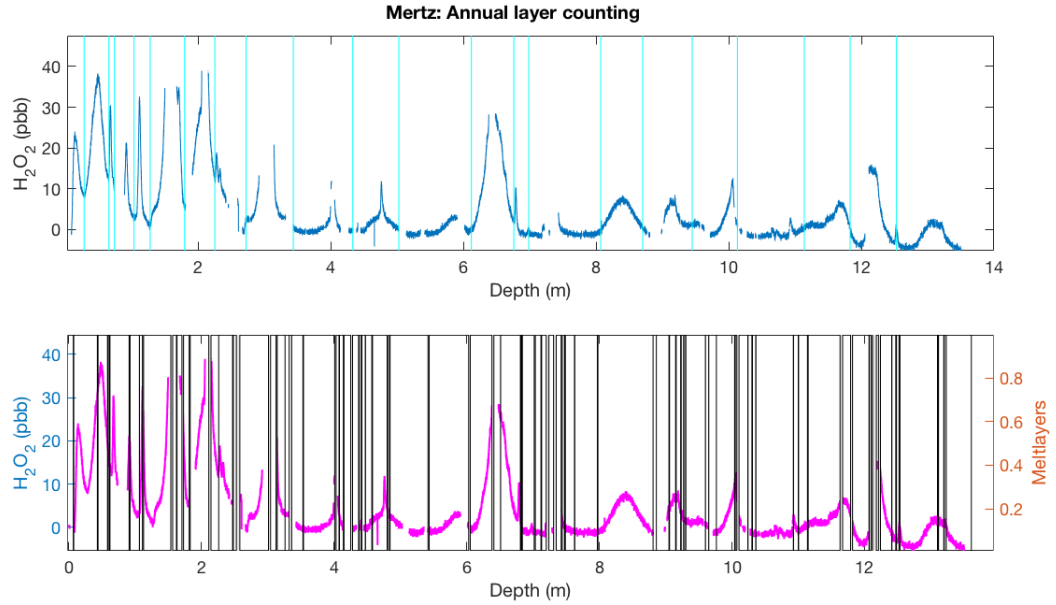

Fig. 26: Counting winter-winter peaks in the Mertz core in the hydrogen peroxide, using the melt layers as a visual aid. The light blue vertical lines are where the winter minima were chosen. Data was only available up to 12.5m, therefore after this we referred to the $\delta^{18}O$ to count the layers

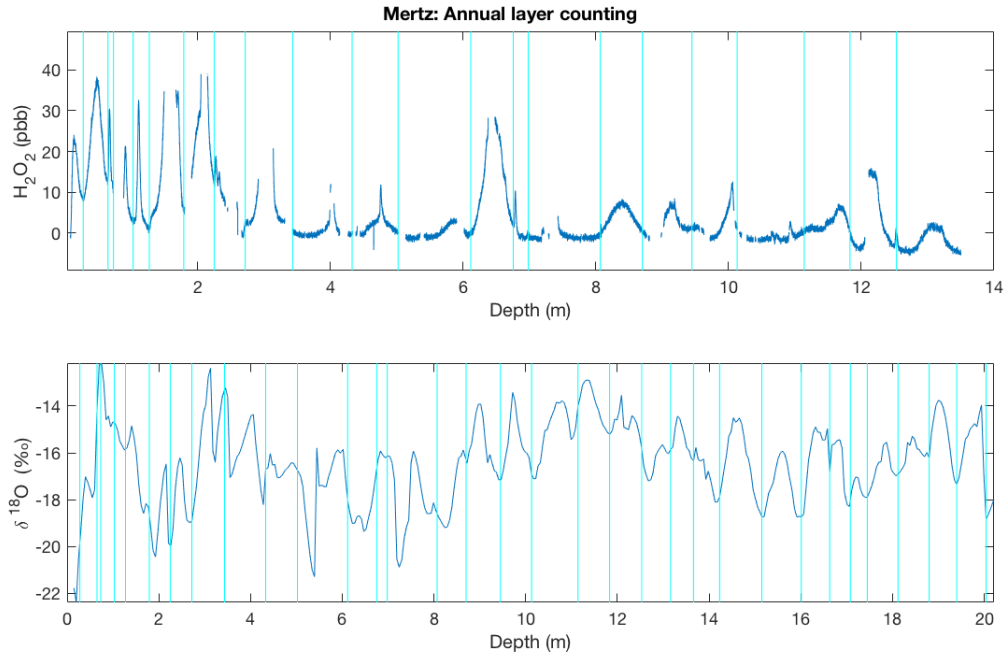

Fig. 27: Counting winter-winter peaks in the Mertz core in the hydrogen peroxide, using the $\delta^{18}O$ as a visual aid. The light blue vertical lines are where the winter minima were chosen. Data was only available up to 12.5m, therefore after this we referred to the $\delta^{18}O$ to count the layers